HHS Public Access

Author manuscript

Biomaterials. Author manuscript; available in PMC 2022 March 01.

Published in final edited form as:

Biomaterials. 2022 February ; 281: 121366. doi:10.1016/j.biomaterials.2022.121366.

Using genetically modified extracellular vesicles as a non-invasive strategy to evaluate brain-specific cargo

David Rufino-Ramos[a,b,c,d,1], **Sevda Lule**[a,1], **Shadi Mahjoum**[a], **Stefano Ughetto**[a], **D. Cristopher Bragg**[a,e], **Luís Pereira de Almeida**[b,c,d], **Xandra O. Breakefield**[a], **Koen Breyne**[a,*]

[a]Neurology and Radiology Department, Massachusetts General Hospital, Harvard Medical School, 13th Street, Building 149, Charlestown, MA, 02129, USA

[b]CNC—Center for Neuroscience and Cell Biology, University of Coimbra, Rua Larga, Coimbra, 3004-504, Portugal

[c]Faculty of Pharmacy, University of Coimbra, Coimbra, 3000-548, Portugal

[d]CIBB–Center for Innovative Biomedicine and Biotechnology, University of Coimbra, Coimbra, Portugal

[e]The Collaborative Center for X-linked Dystonia-Parkinsonism, Massachusetts General Hospital, Charlestown, MA, 02129, USA

Abstract

The lack of techniques to trace brain cell behavior *in vivo* hampers the ability to monitor status of cells in a living brain. Extracellular vesicles (EVs), nanosized membrane-surrounded vesicles, released by virtually all brain cells might be able to report their status in easily accessible biofluids, such as blood. EVs communicate among tissues using lipids, saccharides, proteins, and nucleic acid cargo that reflect the state and composition of their source cells. Currently, identifying the origin of brain-derived EVs has been challenging, as they consist of a rare population diluted in an overwhelming number of blood and peripheral tissue-derived EVs. Here, we developed a sensitive platform to select out pre-labelled brain-derived EVs in blood as a platform to study the molecular fingerprints of brain cells. This proof-of-principle study used a transducible construct tagging tetraspanin (TSN) CD63, a membrane-spanning hallmark of EVs equipped with affinity, bioluminescent, and fluorescent tags to increase detection sensitivity and robustness in capture of EVs secreted from pre-labelled cells into biofluids. Our platform enables unprecedented efficient isolation of neural EVs from the blood. These EVs derived from pre-labelled mouse brain cells or engrafted human neuronal progenitor cells (hNPCs) were submitted to multiplex analyses,

*Corresponding author. Molecular Neurogenetics Unit, Massachusetts General Hospital, 149 Thirteenth Street, Charlestown, MA, 02129, USA. kbreyne@mgh.harvard.edu (K. Breyne).

[1]These authors contributed equally to this work.

Author contribution

D.R.R., S.L., X.O.B. and K.B. conceived and designed the experiments. D.R.R., S.M., S.L., S.U. and K.B. performed the experiments. D.R. R., S.L., S.M. and K.B. analyzed the data. D.R.R., S.L., S.M., S.U., D.C.B., L.P.A, X.O.B. and K.B wrote and edited the paper.

Declaration of competing interest

The authors declare no competing interests.

Appendix A. Supplementary data

Supplementary data to this article can be found online at https://doi.org/10.1016/j.biomaterials.2022.121366.

including transcript and protein levels, in compliance with the multibiomolecule EV carriers. Overall, our novel strategy to track brain-derived EVs in a complex biofluid opens up new avenues to study EVs released from pre-labelled cells in near and distal compartments into the biofluid source.

Keywords

Extracellular vesicles; Brain-derived EVs; hNPCs; Nanoluc; CD63; copGFP

1. Introduction

Cells secrete nanoscopic membrane-derived vesicles, termed extracellular vesicles (EVs). EVs are naturally produced particles surrounded by a lipid bilayer which transport transmembrane proteins at their surface, as well as proteins and nucleic acids in their lumen [1–3]. These vesicles are important mediators of intercellular communication, transferring complex molecular information from one cell to other cells throughout the body [4,5].

EVs can be formed by inward folding of intracellular membranes into endosomes generating intraluminal vesicles (ILVs) that are secreted upon fusion of multivesicular bodies (MVB) with the plasma membrane, typically known as exosomes or by direct outward budding from the plasma membrane, also known as microvesicles or ectosomes [6,7]. To distinguish EVs derived from the plasma membrane or intracellular membrane compartments, tetraspanins such as CD63, CD81 and CD9 are frequently used [8,9]. CD63 has been suggested to be a key determinator for MVB originating EVs as it is highly present in small EVs along with other tetraspanins [10]. Absence of CD63 may exclude EVs of intracellular origin and actively deleting CD63 using CRISPR/Cas9 impairs secretion of MVB-derived EVs, but not plasma membrane-derived EVs [11]. Hence, CD63 tetraspanin has been used to label and track small EVs with endocytic origin in many studies [12–14].

A better understanding of EV content and biomolecule carrier capacity will allow us to explore their potential as biomarkers of disease and as vehicles for treatment. Moreover, EVs released into biofluids by different cells *in vivo* have become an important means to monitor disease status and response to therapy [15–20].

It appears that EVs are mainly retained in the area surrounding the cells of origin and occasionally released into biofluids, such as blood, cerebrospinal fluid, and lymph, thereby reaching distant locations in the body [21,22]. Since EVs derived from many cells in the body can be retrieved in biofluids [23,24] tracing their cell of origin, monitoring their cargo and biodistribution, and determining their fate in recipient cells remain important questions still to be resolved by the EV field. Moreover, the release of EV subpopulations, such as exosomes, microvesicles or apoptotic bodies from the brain reflects their cellular origin, and their relatively low abundance in blood is a major ongoing challenge in the field [25,26]. Nevertheless, RNA and proteins associated with brain derived-EVs can serve as biomarkers for central nervous system (CNS) diseases and have gained increased interest over the years [27, 28]. The mechanism through which EVs pass through the blood brain barrier (BBB) is not yet fully understood, but it has been reported in diseases where the BBB is

compromised - as in the case of glioblastoma [18,29,30]. EVs released within the CNS have also been suggested to be involved in other processes, such as neuronal development [31,32] and neurological disease progression [33,34]. In some neurodegenerative diseases, EVs are believed to facilitate trafficking of misfolded proteins and spreading of the pathology throughout the brain, which is relevant to prion, Alzheimer's and Parkinson's diseases [32,35,36]. The inadvisability of performing brain biopsies in living patients with these diseases has boosted the study of brain-derived EVs in biofluids as a window into the brain [37,38]. However, isolating brain-derived EVs from biofluids is still a challenge due to their heterogeneity and current lack of specific neuronal surrogate surface markers for isolation and understanding their cellular origin [9,39,40].

There are a wide variety of commercial precipitation and affinity kits to isolate EVs from biofluids, such as precipitation kits or tetraspanin (TSN) affinity kits [23,41]. To enrich the sample in brain-derived EVs an additional step of immunoaffinity against neuronal peptides L1CAM or NCAM are typically performed [24,26,40]. However, this method is not completely reproducible and definitive neuronal markers have yet to be identified [39,40].

The aim of our current study was to generate a platform whereby vesicles released from the brain cells into biofluids could be tracked and isolated over time and the EV cargo could be studied to reflect the phenotype of the cells of origin. To this end, we designed a lentiviral vector encoding a CD63 construct, designated here as NoMi (**N**ano-luciferase **o**utside and **M**Cherry **i**nside), based on the position of the tags with respect to the EV compartments. When the NoMi construct is expressed in mice either by brain-engrafted human neural progenitor cells (hNPCs) or locally transduced brain cells, a surface exposed Flag tag on the EVs serves to enable isolation of NoMi-EVs from the blood by affinity-tag capture. This allows analyses of specific transcript and protein levels in brain-derived EVs from peripheral biofluids. Here, we demonstrated the application of the NoMi platform to retrieve both transduced cells and their released EVs *in vitro* and *in vivo* derived from the brain after an affinity pull-down. Additionally, intracranial injections of lentiviral vectors encoding NoMi platform tagged brain-derived EVs were retrieved in blood after affinity pull-down and their associated proteins and transcripts were measured. Moreover, NoMi expressing human neural progenitor cells (hNPCs) were implanted in a mouse brain, and this model was used as a humanized model for detecting passage of EVs out of the brain into the bloodstream. Taken together, these studies emphasize the relevance of the NoMi platform to isolate and detect cargo in pre-labelled brain-derived EVs *in vivo*.

2. Results

2.1. NoMi is designed to tag construct-expressing cells and EVs derived from them

We developed a fluorescent/luminescent hybrid lentiviral construct (6.7 kb genome integrating part and 10 kb total plasmid – see Figure S1) based on the CD63 tetraspanin (TSN) scaffold. CD63 exposes two loops on the outer membrane surface and retains both N and C terminal regions within the EV lumen (Fig. 1A). To enable traceability and a sensitive readout, a 3x FLAG®-tag (DYKDDDK) peptide FLAG®-tag (Flag tag) sequence and Nanoluciferase (Nanoluc) were introduced in the first outer loop of the CD63, displaying them on the outer plasma membrane of the EV donor cell and the EV surface. At the

C-terminus, mCherry was tethered to CD63 exposing it to the cytoplasmic side of cells and the EV lumen (Fig. 1A). To state the position of the detectable proteins with respect to either luminescence or fluorescence, the construct was designated as **N**anoluciferase **o**utside and **m**Cherry **i**nside (NoMi). Moreover, to distinguish engineered cells from the released EVs, an additional copGFP reporter was added to the construct separated by a self-cleaving P2A peptide cleavage site (Fig. 1A). The latter design ensures NoMi and copGFP expression from a single mRNA template under control of the cytomegalovirus (CMV) promoter (Figure S1A). NoMi transduced cells express a diffuse green fluorescence due to cytoplasmic copGFP and punctate pattern of membrane-associated red fluorescence derived from the mCherry tethered to CD63 (Fig. 1B). While the NoMi-copGFP is not actively packaged in EVs, NoMi-mCherry is highly secreted in vesicles. The construct also includes a puromycin cassette that allows drug selection of transduced cells. Overall, the NoMi polycistronic construct takes advantage of the CD63 scaffold to embed multiple readouts for helping discriminate between cells and EVs.

2.2. Affinity pull-down of NoMi expressing cells

As an alternative to puromycin selection, immunoaffinity selection for NoMi expressing cells is an option based on the NoMi-Flag tag. We utilized the exposed Flag tag on the cell surface to develop an antibody-based magnetic affinity protocol upon incubation with commercially available magnetic M2 anti-Flag tag beads. The display of the Flag tag on the outer membrane allows immunoaffinity selection of NoMi cells, as shown in Fig. 2A.

A single cell suspension of NoMi transduced HEK293T cells was incubated with anti-Flag tag affinity beads at room temperature over 1 h on a HulaMixer (Thermo Fisher Scientific), rinsed with PBS and then resuspended with cell media to re-culture NoMi-cells under normal conditions. Bead dissociation was accomplished during a next passage whereby cells were trypsinized off the beads and subsequently exposed to a magnetic field (Fig. 2B). The magnet pulled down the magnetic beads, leaving the dissociated single cells in suspension.

Different types of magnetic beads affected the efficiency of NoMi cell isolation. We tested anti-Flag tag beads (Sigma, M8823), which are 4% agarose beads already bound with anti-Flag M2 (mouse monoclonal antibody) with a 20–75 μm size, and Flag antibody (R&D, IC8529V, monoclonal rabbit) pre-coated Dynabeads (Invitrogen), which are 2.8 μm superparamagnetic beads to pull down Flag tag-expressing cells. In both cases, the beads were successfully attached to the NoMi cells. However, the Sigma beads showed a higher efficiency of NoMi-cell recovery, i.e. 139.3 ± 14.4 cells, whereas 98.3 ± 7.7 cells were recovered with Dynabeads, when copGFP positive cells were evaluated (Fig. 2C). Less debris was also observed microscopically in the anti-Flag M2 group. Taken together, these results demonstrate that this approach is a feasible technique to select and enrich NoMi expressing cells as a preparative step for downstream applications, and anti-Flag M2 magnetic beads should be used for NoMi cell isolation, hereafter referred to as anti-Flag tag beads.

2.3. Affinity pull-down of NoMi expressing EVs

Post-NoMi cell selection, we analyzed the cell media to probe for NoMi expression in EVs (Fig. 3A). First, we removed any residual cells from the conditioned media by centrifugation (300 g for 10 min). The medium was concentrated with 100 kDa spin filters and the total volume reduced down to 500 μl to ensure optimal EV and anti-Flag tag bead contact. Concentrated conditioned media was incubated with anti-Flag tag beads for 1–2 h under rotating conditions at 4 °C. On a magnetic rack, beads were rinsed 3 times in 500 μl PBS to remove unbound contaminants. Depending on the downstream application, a DYKDDDDK elution peptide (same sequence as the Flag tag; Sigma, F3290) was added to dissociate EVs from the affinity beads that bound to the magnetic field (Fig. 3A). We confirmed NoMi-EVs in our resulting Flag tag peptide eluate with transmission electron microscopy (TEM) and nanoparticle tracking analysis (NTA) to evaluate morphology and size distribution of NoMi-EVs, respectively (Figure S2A1 and Figure S2A2). NoMi-EVs displayed a homogenous population with a prominent peak at 159 nm and a traditional EV cup-shaped morphology after fixation. We also found that 75% of the bioluminescence signal of NoMi-Nanoluc was recovered from the beads while 25% remained attached (Fig. 3B).

An additional test was performed to confirm NoMi association with EVs. We applied the NoMi-suspension on a size exclusion chromatography (SEC) column (Fig. 3C). When a non-NoMi control sample consisting of HEK293T conditioned media passes through a SEC column (Fig. 3D1), we observe two peaks, one small fast eluting and one large late eluting peak. The first peak (Fraction 7 to 9) corresponds to EVs, and a second peak (Fraction 14 to 26) corresponds to smaller molecules, predominantly free protein. However, resolving the EV peak from the free protein peak remained difficult due to their overlapping graph profiles (Fig. 3D2). With our bead-based NoMi-EV isolation operation explained above, we were able to improve both detection and size resolution of EVs post-SEC. In short, anti-Flag tag beads incubated with concentrated NoMi-cell media were eluted with the Flag tag peptide, resolved on a SEC column (Fig. 3E1) and subsequently screened for bioluminescence derived from NoMi-Nanoluc as a readout for NoMi-EVs. Fig. 3E2 shows that this procedure resulted in a SEC peak associated with SEC fractions 7 to 9 corresponding to the size range of EVs (yellow graph). However, no peak was visible in the later fractions, implying that NoMi-Nanoluc free protein was non-detectable after our NoMi isolation procedure. To confirm NoMi-Nanoluc association with NoMi-EVs, we disrupted the membrane with a detergent (0.25% Triton X-100 in PBS), washed away all non-NoMi EV components and eluted the NoMi-protein from the Flag tag beads (Fig. 3E1). The resulting Flag peptide eluate was passed through the SEC column and investigated for NoMi-Nanoluc. We observed a shift in bioluminescence detection to the later SEC fractions (Fraction 14 to 26) post-detergent treatment of NoMi-EVs (dark grey graph in Fig. 3E2). This change in NoMi-Nanoluc SEC profile change confirms the association of NoMi-Nanoluc with intact NoMi-EVs in the yellow graph and NoMi-Nanoluc with free protein in the grey graph.

In conclusion, the NoMi construct is selectively associated with EV membranes in biofluids. We can distinguish both intact as well as lysed EVs through the NoMi-Nanoluc component in our construct. A downstream laborious SEC separation has little added value in EV purification after Flag tag pulldown of intact NoMi-EVs.

2.4. NoMi-EVs carry both NoMi associated proteins and exRNAs

In this section we wanted to assess markers, such as proteins and exRNAs transported by our engineered NoMi-EVs. At the protein level, NoMi-EVs carry Nanoluc and mCherry labels for luminescent and fluorescent detection, respectively. Both NoMi-labels were found to be part of a single 81.1 kDa NoMi-protein as determined by Western Blot analysis using specific Nanoluc and mCherry antibodies on NoMi-EV samples (Fig. 4A1). Non-NoMi EVs were used as a control sample and anti-Hsp70 as an EV loading control.

To evaluate the integrity of NoMi-EVs and the orientation of the NoMi proteins at the EV membrane, we incubated the vesicles with proteinase K for outer EV tethered NoMi-Nanoluc, and with proteinase K plus 0.25% Triton X-100 for NoMi-mCherry on the inner EV surface. NoMi-Nanoluc luminescence decreased more than 99% when NoMi-EVs were exposed to proteinase K for 30 min at 56 °C (Fig. 4A2), in contrast to the NoMi-mCherry fluorescent signal which showed less than 4% loss (Fig. 4A3), suggesting that NoMi-mCherry protein is protected inside of EVs. A significant drop of 14% was observed though an additional disruption of the EV membrane with 0.25% Triton X-100 for 30 min, which allows penetrance and degradation of proteins inside of EVs by proteinase K (Fig. 4A3). This confirms that NoMi-mCherry is protected by the EV membrane while NoMi-Nanoluc is exposed on the outer membrane surface. Of note, NoMi proteins should be measured at physiological conditions, as both NoMi-Nanoluc and NoMi-mCherry are affected by pH and their detection would be impaired in conditions lower than pH6 (Supplementary Figure S2B).

To analyze our NoMi-mCherry EV content protected by the EV membrane layer, NoMi-EVs were applied to an ExoView Tetraspanin chip (NanoView Biosciences) that tethers single EVs to a surface with arrayed antibodies against CD63, CD81, and CD9 and IgG (negative control) (Fig. 4A1) [42–44]. Label free capture of NoMi-EVs against each TSN (CD81, CD63 and CD9) was performed and then co-localized with the NoMi-mCherry signal. mCherry signal was positive for 69% of NoMi-EVs expressing at least 1 molecule of CD63, 30% expressing at least 1 molecule of CD81 and 16.5% expressing at least 1 molecule of CD9 particles (Fig. 4B2). EVs sized between 60 and 90 nm showed a tendency to have a positive correlation comparing their NoMi-mCherry content to their size given by the equation $\log10(Y) = 0.00642X+2.234$, but this was minimal given the small correlation coefficient $R2 = 0.2684$ (Fig. 4B3).

Along with proteins, RNA fragments are transported by EVs, also termed exRNA [45]. Here we explored whether NoMi construct-encoded exRNAs can be amplified thereby lowering the signal to noise ratio seen with NoMi-proteins, such as NoMi-Nanoluc (Fig. 4C). We observed that the NoMi-Nanoluc bioluminescent signal dropped 99% after diluting the sample 1000 times to reach the noise level.

Our NoMi-construct does not contain an EV packaging signal and encoded both copGFP and NoMi on a single mRNA (Fig. 1A). Still, copGFP and NoMi-Nanoluc RNAs (or fragments from them) were detected to similar extend in cells with a Ct = 16 (Figure S2C2) and in NoMi-EVs (Fig. 4D1) with a Ct = 32. We also verified that non-NoMi

encoded exRNAs were co-transported with NoMi-EVs. Indeed, GAPDH, a well-known house-keeping gene, was also detected in NoMi EVs with a Ct = 32 (Fig. 4D2).

We evaluated the ability of copGFP exRNA in NoMi-EVs as an alternative tool for EV detection and a normalization factor for rare RNA events. Specific NoMi-TaqMan probes (see methods) were designed to detect trace amounts of copGFP-exRNA with droplet digital PCR (ddPCR). The samples screened for NoMi-Nanoluc bioluminescence in Fig. 4C were used for RNA extraction, cDNA synthesis, and cDNA amplification for ddPCR analysis. ddPCR detection with specific copGFP-exRNA TaqMan probes dropped 57.2% under the same conditions (Fig. 4D2). Our data also indicates that detection of copGFP-exRNA in NoMi-EVs supersedes GAPDH exRNA detection, whereas under the same conditions the latter dropped by 93.1% (Fig. 4D2). It could be partially caused by a smaller copGFP amplicon when compared to GAPDH (Figure S2 C1).

Taken together, the NoMi construct can be used to detect and monitor fingerprint biomolecules in EVs derived from donor cells. We have shown that NoMi-EVs transport NoMi construct encoded proteins, such as Nanoluc and mCherry, and non-encoded proteins, such as CD63, CD9 and CD81, as well as NoMi construct encoded exRNAs, such as for Nanoluc and copGFP and non-encoded exRNAs, such as GAPDH. Overall, copGFP exRNA detection can be used as a sensitive fingerprint in complex and low abundant samples of NoMi-EVs.

2.5. NoMi enables the detection of EV-producing brain cells in living mice

We next determined whether the NoMi-construct enables EV detection from membrane-enclosed compartments, such as brain. We intracranially injected lentivirus encoding the NoMi construct to stably transduce brain cells in the striatum of mice and tried to detect NoMi-Nanoluc expression in accordance to recent reports that raised the possibility of using Nanoluc to study EVs *in vivo* [46,47]. Unfortunately, we were not able to detect a reliable bioluminescent NoMi-Nanoluc signal after retro-orbital administration of furimazine, which is the Nanoluc substrate, 7 days post-intracranial injection of the NoMi lentivirus vector. To boost our NoMi-Nanoluc detection in the brain, we tested fluorofurimazine, a new modified furimazine substrate with better lipophilic properties. Hereby, a robust luminescent signal was observed in the brain (Fig. 5A1) after intraperitoneal (IP) administration of 100 µl of 2x diluted fluorofurimazine (Nano-Glo® *In Vivo* Substrate, Promega®) according to manufacturer instructions. The optimal luminescence/background ratio was obtained 5 min after administration of this substrate (Fig. 5A2) and remained stable for at least 10 min.

To confirm our *in vivo* bioluminescent results, expression of the NoMi construct was verified in brain cells with immunofluorescence staining of coronal brain sections 13 days after injection. In Fig. 5B, we demonstrated that other labels of the NoMi construct, such as copGFP, mCherry and Flag, were detectable by immunofluorescence staining. NoMi-copGFP was visualized (in the Cy2 channel) at the injection site in the striatum. In the same region, we also detected the CD63-associated labels – NoMi-mCherry (in the Cy3 channel) and the NoMi-Flag tag (in the Cy5 channel) upon immunostaining with anti-Flag tag antibody (Sigma) (Fig. 5B1). Moreover, 11.5% of the striatal region was transduced

with lentivirus encoding the NoMi construct, showing the well-defined localization of the NoMi-lentivirus vector injection (Fig. 5B2).

Taken together, these findings suggested that our NoMi platform provides readouts that can be used to monitor NoMi expression in the brain of a living mouse.

2.6. Brain-derived NoMi-EVs are released into the bloodstream

As described in the previous section, NoMi expression is predominantly restricted to the injection site in the striatum of mice 13 days after injection. We explored whether NoMi-Nanoluc activity in the brain spreads from the initial NoMi-Lentivirus injection site (Fig. 6A1). For this method, each sample was taken with 40 μm intervals and contained 80 μm of brain tissue corresponding to 5 adjacent coronal brain sections of 16 μm each. We observed at the injection site of the NoMi-Lentivirus injected mice a 3-fold higher luminescence signal peak in comparison to the 1% PBS/BSA injected control mice. A spatial gradient resulting from a combinatory effect of the initial NoMi Lentivirus injection and spreading of the NoMi-EVs from sites of transduction could also be visualized. We observed detectable levels of NoMi-Nanoluc as far as 800 μm away from the injection site in both anterior and posterior directions corresponding to 1-fold difference comparing to the control animals injected with 1% PBS/BSA (Fig. 6A2). The background luminescence signal from the control samples was between 200 and 300 RLU and did not vary throughout the entire striatum.

To investigate the ability of NoMi-EVs to be released into the bloodstream from brain, we evaluated whether NoMi-Nanoluc bioluminescence was detectable outside the brain compartment. To retrieve NoMi-EVs in blood we collected 1.5 mL of blood from mice into EDTA treated tubes at the time of sacrifice and maintained under agitation. Blood cells were removed upon 2 × 300 g for 10 min and serum was incubated in 4 °C for at least 24 h with anti-Flag tag beads to capture NoMi-EVs (Fig. 6B1). After affinity pull-down, the NoMi-Nanoluc bioluminescent signal in the NoMi-EVs sample was evaluated (Figure S3A). NoMi-EVs showed a mean of 597.0 ± 51.3 RLU while control had a mean of 412.7 ± 80.6 RLU, however the result was not significantly different (p *value* = 0.086) (Figure S3A). To improve the sensitivity of the method, we analyzed the NoMi-copGFP exRNA in NoMi-EVs by ddPCR (Fig. 6B2). NoMi EVs contained 116.2 ± 17.0 copies copGFP/ul compared to 26.70 ± 12.88 copies copGFP/ul in the control samples, indicating a significant increase in expression (p *value* = 0.011) (Fig. 6B2). Since the only source of copGFP exRNA is from NoMi injected striatum, the result suggests EVs captured by affinity pull-down in serum are derived from the brain.

We also analyzed the peripheral organs in control and NoMi mice after perfusion with PBS to remove NoMi EVs present in the blood. The NoMi-Nanoluc bioluminescence signal was not significantly different between our conditions (Figure S3A). CopGFP-exRNA levels were also not significantly different within the peripheral organs (Figure S3B), suggesting no EVs accumulation, uptake below detection level or degradation of exRNA post-uptake.

Our data suggests that brain cells can secrete EVs in the brain compartment and in the blood. Our NoMi technique makes use of EVs as multibiomolecule carriers to detect spread

of EVs in close proximity (NoMi-Nanoluc bioluminesence) and far distal compartments (copGFP-exRNA).

2.7. NoMi-hNPC engraftment as a relevant humanized mouse model for EV spreading from the brain compartment

Viral particles can potentially spread throughout the brain and infect other cells in the bloodstream. To show that EVs spreading to the bloodstream is not solely derived from locally transduced cells but can also be observed for brain-implanted human cells, we stably transduced primary human neural progenitor cells (hNPCs) with the NoMi vector *in vitro* prior to implantation into mouse brains. In line with our previous observations, expression of the NoMi vector in hNPCs was demonstrated by expression of both copGFP and mCherry in culture (Fig. 7A). hNPCs-derived NoMi-EVs were harvested from 500 μl final volume of concentrated conditioned media from 100,000 hNPCs, as indicated in Fig. 3A and presence of NoMi-EVs was verified comparing media from NoMi-positive and NoMi-negative hNPCs, in the last condition control EVs were isolated by SEC. CopGFP-exRNA was only detected in engineered hNPCs-derived EVs, mean ± SEM 0.95 ± 0.22 compared to control EVs, mean ± SEM 0.00025 ± 0.00025, (p *value* = 0.0048) (Fig. 7B), supporting its use as a sensitive reporter to detect EVs from humanized cells.

NoMi expression was retrieved in the brain 7- and 14-days post-engraftment with immunofluorescence through the three NoMi hallmarks copGFP, mCherry and Flag in the Cy2, Cy3, and Cy5 channels, respectively (Fig. 8B). Based on our immunostaining results, there was an increase in NoMi related protein signals over time in mouse brain sections from day 7 vs day 14 post-implantation of NoMi-hNPCs. To determine if this increase reflected proliferation of the engrafted NoMi-hNPCs, we assessed the cell cycle status of NoMi-hNPCs in the mouse brains based on Ki67 staining in both day 7 and day 14 post-implantation groups (Fig. 8C) which indicated active cell division by the grafted cells. In spite of this proliferative capacity, the cell source of NoMi-expression remained localized which was similar to our previous results in lentiviral induced NoMi expression in endogenous mouse brain cells. We also showed that all the proliferative engrafted NoMi-hNPCs were still expressing the human nuclear antigen (hNA) (Fig. 8C). Moreover, the copGFP expressing NoMi-hNPCs retained their neuronal lineage commitment at early progenitor stage as shown through the expression of Pax6 and Nestin which are neuroectoderm markers for cells in an early neural progenitor and non-differentiated state [48,49] (Fig. 8D).

NoMi-hNPCs were recovered from the brain 14 days after implantation. The animals were sacrificed, and brain samples were used to obtained 2 mm-thick coronal sections having the injection site in the middle of the section. Then the coronal sections were dissociated into a single brain cell suspension and after 300 g 10 min spin, cell pellets were incubated with anti-Flag magnetic beads following the isolation protocol described in Fig. 9A.

The success of NoMi-hNPCs recovery was evaluated by copGFP-exRNA analysis. Mouse brains lacking NoMi-hNPCs had no detectable copGFP-exRNAs following the same isolation method whereas the exRNA in the NoMi-hNPCs engrafted brain sections could be detected with a 0.04 copGFP/GAPDH ratio (Fig. 9B).

After establishing survival, proliferation, and stem cell characteristics of our NoMi-hNPCs within the brain, we investigated whether hNPCs derived NoMi-EVs were released into the periphery. We applied the isolation operation described in Fig. 3A to the blood samples of NoMi-hNPC engrafted mice at 7- and 14-days post-implantation. Following this method, copGFP-exRNA detection was used to confirm NoMi-EV presence in serum. copGFP-exRNA was not detected in control samples, while an increased amount from 1 to 3.5 of copGFP/GAPDH ratio was observed comparing 7 days vs 14 days after hNPCs implantation, suggesting copGFP-exRNA levels in NoMi-EVs correlates with increased number of NoMi-hNPCs detected in the mice over time (Fig. 9C).

Taken together, our results confirm with a non-invasive humanized mouse model that EVs can spread from the brain to the blood. Our NoMi construct has no observable effect on cell morphology post-implantation in the brain but has an added value in EV population isolation and characterization in distal body compartments.

3. Discussion

NoMi is a platform to study non-cellular long-range communication in animal models. In this respect, we evaluated NoMi reporters in different models in the brain, a membrane-enclosed compartment known to have selective permeation. Characterization of NoMi-EVs released into the bloodstream emphasized the lack of sensitivity and robustness when relying only on conventional single biomolecule detection methods for interorgan EVs communication and highlighted the usefulness of platforms such as NoMi that ensure multiplex analysis of EV-mediated cargo transfer.

The flexibility and usability of the NoMi-construct arises from its labels. The NoMi abbreviation '**N**anoluc **o**utside and **m**Cherry **i**nside' results from the expression of the endogenously loaded cargo at different sides of the EV membrane. The targeting of NoMi to EVs was pursued through tagging of TSNs. TSNs are proteins heavily enriched in EVs, and the most abundant ones are CD81, CD9 and CD63; hence their usefulness as EV markers [9,50]. A CD63 scaffold (25 kDa) was provided with cargo enabling bioluminescence and fluorescence detection in addition to affinity pulldown resulting in an 81.1 kDa NoMi fusion protein. The transmembrane spanning nature of CD63 allows contact between the outer exposed and the lumen side of EVs and is being commonly used for engineering purposes [12,51–53]. CD63 exposes two loops on the solvent exposed side of the membrane, while the N and C termini are protected in the lumen of the EVs [8]. It is reported that the first loop of CD63 is not glycosylated and open for mutation or integration of sequences, in contrast to the second loop [54]. Consequently, the first CD63 loop is more lenient to genetic manipulation, including incorporation of NoMi-Nanoluc and NoMi-Flag tag labels. The second loop was avoided as it is a conserved CD63 region that can become more antigenic due to post-translational sugar moiety additions enabling anti-tetraspanin antibody development and detection [55,56]. The N- and- C termini are commonly used to fuse proteins, such as GFP [12,53] or luciferases [51,57,58] while protecting them by the EV membrane. Similarly, NoMi-mCherry was attached to the C-terminus of the CD63 scaffold.

NoMi-Flag tag displayed on the membrane surface allows affinity-based capture to isolate either NoMi-expressing cells and their NoMi-EV progeny. NoMi-Flag at the cell surface results from fusion of MVBs with the plasma membrane [59]. CD63 including other TSNs involved in the endosome pathway are enriched in MVBs, which contain exosomes [3]. Upon exosome release, the MVB membrane gets exposed at the cell surface allowing affinity pull-down of NoMi expressing cells as an attractive alternative selection method to antibiotic or fluorescent cell selection by NoMi construct encoded puromycin and copGFP, respectively. Affinity pull-down of cells is an accepted selection method for cell enrichment [60,61]. However, release of cells from affinity beads is cumbersome and critically dependent of the eluent. Others have shown that recombinant DYKDDDDK peptide necessary to dissociate cells from anti-Flag tag beads can be cytotoxic [62]. Therefore, Flag tag peptide elution was avoided, and cell dissociation from beads was accomplished during cell passaging with trypsin and magnetic bead depletion. We hypothesize that mild trypsinization mainly affected the anti-Flag tag antibody bound to the magnetic beads as our Flag tag was embedded in a CD63 structure and thus more resistant to proteases than tags at the solvent exposed N and C terminal ends of EV targeting proteins [63].

Next to cells, NoMi-EVs isolation could be guaranteed through specific NoMi-operations. To isolate NoMi cells an affinity selection was performed from the pellet obtained after centrifugation at 300*g* for 10 min, while for NoMi-EVs isolation affinity selection was performed from the supernatant cell media. Our construct also allows for an additional quality control step to distinguish between engineered cells and their derived EVs after isolation. As a cell trait we included copGFP and uncoupled its expression by a posttranslational self-cleavage site from our CD63-like NoMi protein which had a high EV association tendency. CopGFP was chosen over eGFP because of its quaternary structure (~104 kDa) in mammalian cells [64–67]. Compared to monomeric eGFP (26.9 kDa), the bulky format of copGFP reduces its chance of being packaged as a protein in NoMi-EVs, favoring its retention in the cytosol. Indeed, our fluorescent images showed NoMi-coupled mCherry as being punctated in our NoMi-cells, a distribution pattern typically linked to MVBs and their EVs [68], in contrast to the disperse cytoplasmic copGFP phenotype [65].

The NoMi platform anticipates one of the major challenges in the EV field which is the limited capacity to capture EVs from specific tissues in biofluids and analyze their content [25,26]. There are a wide variety of commercial precipitation and affinity kits to isolate EVs from biofluids. Precipitation kits, such as ExoQuick are commonly used to isolate EVs from all types of body fluids. However, the EVs collected are typically impure and very heterogeneous [9]. To reduce the heterogeneity of isolated EVs, affinity kits targeting specific EV hallmarks, such as the TSNs CD9, CD81 and CD63 are also used [10,50]. In order to specifically isolate brain-derived EVs, a commercial kit followed by immunoaffinity pulldown against a neuronal peptide such as L1CAM or NCAM has been used [69,70]. However, these proteins are not uniquely expressed in the brain, and they can also be released as free proteins, causing some controversy in the field [24,26,37]. Despite the large number of isolation methods and studies focusing on analysis of brain-derived EVs under healthy and diseased conditions, there is an absence of suitable capture and readout systems to trace back the origin of EVs and specifically analyze these limiting amounts of sample. Here, we showed that pre-labelled brain-derived NoMi-EVs can be captured from biofluids

by affinity anti-Flag tag selection while tracking back their cellular origin and providing information about the ongoing state of their source cells. Therefore, while NoMi-EVs are trackable, we still face the problem of identifying EVs released from non-pre-labelled resident brain cells.

We detected our NoMi-EVs with NoMi-mcherry, NoMi-Nanoluc and NoMi-exRNA through *in vitro* fluorescence quantification and Exoview, bioluminescence *in vitro* and *in vivo*, and ddPCR analysis, respectively. MCherry fluorescence is restricted by the number of single proteins that can be excited, hence the limited use of NoMi-mCherry in EVs. Although this can be verified with very sensitive detection systems such as ExoView Tetraspanin chip (NanoView Biosciences), a single EV resolution technique arrayed with antibodies against TSNs – CD63, CD81, and CD9 [42–44] with an IgG isotype used as a negative control [42–44]. This technique binds individual EVs to each antibody spot and their size is measured by high-resolution interferometric imaging of single EVs in a suspension [42]. Interestingly, we did not observe a strong correlation between NoMi-EV size and NoMi-mCherry fluorescence intensity. This can be reasoned as our NoMi-EVs are thought to originate from endocytic compartments known to produce a homogenous population of vesicles with less capacity to fluctuate their size and thus their cargo, as compared to those derived from the plasma membrane [71,72].

This is in contrast to fluorescent-loaded EVs generated with membrane-associated labels like PalmGFP or PalmtdTomato [73,74] which tag different EV-species at once with a broader EV-size range [75].

To increase our detection sensitivity of NoMi-EVs, NoMi-Nanoluc was utilized. One luciferase protein such as NoMi-Nanoluc can turn over multiple substrate molecules. Nanoluc was preferred over other luciferases due to its small size of 19.1 kDa, high signal-to-noise ratio, no need for ATP and Mg^{2+}, and more than 150-fold increase in luminescence compared to other common luciferase systems (England, Ehlerding, and Cai 2016). These characteristics made Nanoluc ideal to embed in our CD63 scaffold and hereby develop a highly sensitive quantitative luminescent readout to study EV secretion.

Both NoMi-Nanoluc and NoMi-mcherry were found to be affected by pH environments lower than 6, limiting their observation in acidic endosomes in NoMi-cells. This NoMi-characteristic that benefits EVs over cell detection has been extensively used for EV-secretion detection with pH sensitive fluorophores such as pHluorin-CD63 [68,76]. To counteract the pH limitations of EV detection while boosting the sensitivity of our NoMi-platform, we explored whether the NoMi-exRNA could be detected and amplified, increasing signal to noise ratio and overcoming stoichiometry problems observed with protein detection methods. ExRNA carried by EVs consists of small RNAs, including fragmented or degraded mRNA and short RNA species, typically <3 kb [45,77]. In accordance with questions raised by the field whether exRNA species without known active EV packaging signals can be packaged by brain cells into EVs and then released from the brain compartment, we focused on copGFP-exRNA detection. As mentioned above, copGFP protein appears to have a lower tendency to be packaged into NoMi-EVs in contrast to NoMi-mCherry and NoMi-Nanoluc. Notwithstanding copGFP-exRNA does not contain a

known active EV packaging signal in its 663bp sequence, it appears to have an advantage in exRNA-EV loading. Possibly because its cDNA is positioned rather in the middle of our 3.7 kb NoMi-construct and hereby less prone to degradation at the extremities where NoMi-mCherry and NoMi-Nanoluc cDNAs are situated [64,78].

The study of EVs *in vivo* is challenging, particularly because fluorescent labels such as copGFP or mCherry are not regularly used to monitor expression in living mice due to high autofluorescence, whereas luciferase-based reporters are commonly used for *in vivo* bioluminescence imaging upon substrate administration (England, Ehlerding, and Cai 2016; [79]. Firefly, *Renilla* and *Gaussia* luciferases are the most used for bioluminescence signal detection [63,73,79,80], while Nanoluc was recently reported for study of EVs *in vivo* [46,47]. Some concerns arise with *in vivo* Nanoluc detection because the signal wavelength of 460 nm, limits deep penetrance in tissues and the substrate needs to cross the blood brain barrier, both essential for visualizing small bioluminescent events in the brain [81]. We overcame this by using fluorofurimazine, an optimized substrate for *in vivo* purposes more permeable to BBB and brighter than furimazine [82]. NoMi-Nanoluc bioluminescence was used to monitored stable transduction of brain cells with lentivirus encoding the NoMi construct.

Intracranial injection of lentivirus is typically well retained at the injection site in contrast to adenoassociated virus (AAV) vectors that can spread to other regions and cross the BBB [83,84]. Taking this into consideration, we detected NoMi-Nanoluc signal that peaked at the injection site and could still be detected 800 μm away from the injection site. This observation suggests a spatial gradient resulting from a combinatory effect of transduced cells in the injection site and brain-derived NoMi-EVs at distant regions. We did not expect to detect lentivirus vector within the brain 13 days after injection, since they cannot replicate and their described half-life in culture is less than 48 h [85]. Due to the presence of a ubiquitous promotor, such as CMV, we cannot conclude yet which cells are communicating through NoMi-EVs. However, a similar study used the specific neuronal promoter CaMKII demonstrated neuron to astrocyte communication 500 μm away from the injection site using a floxed CD63-GFP mouse model activated upon intracranial injection of AAV8 expressing CaMKII-Cre [86].

To counter limitations of potential virus spreading from the injection site, NoMi-transduced NoMi-hNPCs were implanted into the brain and the signal from NoMi-EVs was evaluated. From the five hNPCs lines transduced with the construct, only two of them expressed copGFP and mCherry markers after puromycin selection. We postulate that some lines turned off the CMV promoter as it is known to happen in embryonic cells [87], thus changing the promoter in the future may improve the expression in these cell lines. Moreover, alternatives to copGFP protein can be considered as it has been linked to needlelike aggregates in mammalian cells that might be toxic for hNPCs [66]. After implanting of NoMi-hNPCs, the engrafted cells were able to survive and proliferate, suggesting interaction between mouse brain cells and the xenotrans-plant. Indeed, hNPCs grafts have been used in cell replacement strategies, promoting neurogenesis and neuroprotective effects in diverse neurologic diseases [88,89]. Interestingly, part of their beneficial effect has been described to be related to the release of EVs [89–91].

Both mouse models demonstrated that NoMi-EVs produced in the brain cross the BBB and can be retrieved in serum. However, the number of EVs derived from brain grafts in the serum are low [38] which further limited the analysis of our EV sample. The rapid and selective isolation of NoMi-EVs with Flag tag affinity pull-down aids in concentrating our sample prior to RNA isolation and subsequent highly sensitive ddPCR analysis. In our reporter model, EVs in the blood contained copGFP-exRNA that could only be derived from the brain, the biosource of copGFP-exRNA. Of note, our NoMi operation proved to be sensitive enough to detect copGFP-exRNA in EVs, even without an EV packaging signal. This could be important for future applications as disease relevant markers often lack known EV specific packaging signals and therefore may not be actively packaged into EVs.

In conclusion, the NoMi platform we developed presents an additional advantage to the field as it can be used to detect and track back brain-derived EVs in complex organs and biofluids originated from pre-labelled cells within the mouse brain.

4. Methods

4.1. Plasmid cloning

The vector (Addgene #73037) encoding for copGFP, puromycin and nanoluc was restricted with *Bam*HI and *Xba*I and used as backbone for a Gibson assembly (New England Biolabs) to insert a gBlock (IDT) encoding for the N-terminus of NoMi (see Figure S1b). The resulting plasmid was restricted with *Bmg*BI and *Bar*I to incorporate the NoMi C-terminus with Gibson assembly and generate the NoMi plasmid.

Each assembly reaction contained approximately 100 ng insert and 50 ng expression vector and was incubated at 50 °C for 30 min - 4 h following the manufacturer's protocol. The plasmids were transformed into NEB® 10-beta Competent *E. coli* (High Efficiency) (New England Biolabs) and overnight grown at 37 °C on antibiotic containing agar plates [10 mL Bacto agar (Sigma) with LB medium in a 60 mm dish]. Single colonies were picked, grown in LB broth (Sigma) and extracted using a QIAprep Spin Miniprep Kit (Qiagen). To confirm correct insertion, a restriction digest was performed, and fragments electrophoresed in a 1.5% agarose gel and stained with GelRed (Biotium). Images were acquired under UV light using Azure Biosystems c300 Image. When correct profiles were detected, complete plasmid sequencing using Next-Generation sequencing technology (MGH CCIB DNA Core) was performed to validate plasmid integrity.

4.2. Lentiviral production

Lentiviral vectors encoding the NoMi construct (Fig. 1 and Supplemental Figure 1) were produced in HEK293T cell line with a three-plasmid system, following Addgene recommendations. Briefly, cells were seeded and 24 h after, transfected with psPAX2 (Addgene plasmid #12260) and pMD2.G (Addgene plasmid #12259) packaging plasmids and NoMi plasmid. 6 h upon transfection cells were washed with PBS and media was replaced. Lentiviral isolation was performed 48 h later upon ultracentrifugation at 70 000 g and the pellet was re-suspended in 1% PBS/BSA [92]. The viral particle content was

evaluated by assessing HIV-1 p24 antigen levels by ELISA 2.0 (Retro Tek, 0801002). Concentrated viral stocks were stored at −80 °C until use.

4.3. Generation of stable HEK293T and human-neural progenitor cell (hNPC) lines

hNPCs were derived from hIPSCs as previously described by our lab [93]. NPCs at passage >9 and no more than 20 were used for experiments. HEK293T cells and hNPCs were transduced 24 h after plating with Lentiviruses encoding the NoMi construct (400 ng of P24 per 200, 000 cells). At 24 h later, the medium was replaced with regular medium and cells were cultured and expanded in their standard conditions. Puromycin selection was performed and endogenous fluorescence of copGFP and mCherry was monitored regularly.

4.4. Isolation of stable HEK293T cells by magnet-activated cell sorting (MACS)

In order to select the more efficient magnetic beads for isolating the stable HEK293T cells via 3x FLAG®-tag (DYKDDDK) peptide (F4799, Sigma) (Flag tag), MACS was performed by using two different magnetic beads (Fig. 2); anti-flag M2 magnetic beads (Sigma, M8823) are 4% agarose beads already bound with anti-Flag M2 (mouse monoclonal antibody) and Flag antibody (R&D, IC8529V, monoclonal rabbit) pre-coated Dynabeads (Invitrogen, 11203D, sheep anti-rabbit IgG) are 2.8 μm superparamagnetic beads magnetic beads with affinity-purified polyclonal sheep anti-rabbit IgG covalently bound to the bead surface. Transduced HEK293T cells were incubated with magnetic beads at room temperature over 1 h on a HulaMixer (Invitrogen, 15920D) and then the cell-bound magnetic beads were isolated by using a magnetic rack, DynaMag-2 Magnet (Invitrogen).

4.5. Size exclusion chromatography (SEC) for extracellular vesicle (EV) isolation

Conditioned medium was collected from cells with 80% confluency from 100 mm plates after 72 h (seeding density 2.2×10^6 cells/plate) and centrifuged at 300×*g* for 5 min to remove cellular debris. Medium was then concentrated with UFC9100 Amicon® Ultra-15 Centrifugal filters to a final volume of 0.5 mL (spin at 6000×*g* for 15 min). Concentrated media was passed through IZON qEV original size exclusion columns according to the manufactures protocol. Five-hundred-microliter fractions were collected. High particle/low protein fractions (from 7 to 11) were collected and pulled in Amicon®Ultra-0.5 Centrifugal filters to a final volume of 100 μl.

4.6. Affinity beads for EV isolation

Conditioned medium was collected from cells with 80% confluency from 100 mm plates after 72 h (seeding density 2.2×10^6 cells/plate) and centrifuged at 300×*g* for 5 min to remove cellular debris. Medium was then concentrated with UFC9100 Amicon® Ultra-15 Centrifugal filters to a final volume of 0.5 mL (spin at 6000×*g* for 15 min). Concentrated media was incubated with 10 μl anti-Flag M2 beads (Sigma, M8823) (≥0.6 mg/mL binding capacity) on a HulaMixer under gentle shacking for at least 1 h at 4 °C. Beads containing EVs were pulled down and washed 2x with PBS. EVs release from beads occurs after incubation with M2 peptide at least 1 h 4 °C.

4.7. Single EV analysis with exoview

EVs were obtained from NoMi transduced HEK293T cells through SEC and concentrated with spin filter columns (milipore 30 kDa) to a final volume of 30 μl. According to the guidelines provided by (NanoView Biosciences, USA), the samples were incubated on the ExoView Tetraspanin Chip for 16 h at room temperature. After washing the chips three times in 1 mL PBS for 3 min It was performed a free label imaging with the ExoView R100 reader. Procedure and analysis were performed by the ExoView representative.

4.8. Western Blotting

HEK and Nomi EVs were boiled at 95 °C for 10 min and the concentration was determined using Pierce BCA Protein Assay Kit (Thermo Scientific Pierce, Rockford, IL,USA). Then 25 μg of each sample was resolved by electrophoresis on 4–12% SDS-PAGE in Bis-Tris Plus (Thermo Scientific Pierce, Rockford, IL,USA) at 120 V. Next, the proteins were transferred to polyvinylidene fluoride membranes (PVDF) using the Invitrogen iBlot 2 Dry Blotting System. Membranes were blocked by incubation in 5% non-fat milk powder in 0.1% Tween 20 in Tris buffered saline (TBS-T) and incubated overnight at 4 °C with primary antibody against HSP-70 (1:500 Santa Cruz Biotechnology, D1519), Nanoluc (1:500, Promega, N700A), RFP (Thermo Fisher, MA5–15257) at 4 °C overnight. Then, the membranes were washed 3 times with TBS-T for 10 min and incubated with a secondary antibody (1:2500) at RT for 1 h. Membranes were then washed with 3 times TBS-T for 10 min. Bands were visualized by Pierce™ ECL Western Blotting Substrate (32106) in the Azure Biosystems C300 imaging equipment.

4.9. Animals

All animal experimental protocols were approved by the Massachusetts General Hospital Institutional Animal Care and Use Committee. C57BL/6, BALB/c and NU/NU Nude mice (Charles River Laboratories) were maintained with unlimited access to water and food under a 12-h light/dark cycle. Male and female mice ranging from 8 to 10 weeks in age were randomly assigned to experimental groups.

4.10. Stereotaxic injection into the mouse brain

Mice were stereotaxically injected into the right striatum (anteroposterior: +0.6 mm, lateral: 1.8 mm, ventral:−3.3 mm) with concentrated lentiviral vectors in a final volume of 4 μl containing 400 ng of p24 antigen or transduced hNPCs with 100,000 cells in 5 μl opti-MEM reduced serum medium (Gibco, 14362) at an infusion rate of 0.25 mL/min using a 10 mL Hamilton syringe. Control animals were injected with 4 μl of 1%PBS/BSA or 5 μl of opti-MEM. 5 min after the infusion was completed, the needle was retracted 0.3 mm and allowed to remain in place for an additional 3 min prior to its complete removal from the mouse brains [94].

4.11. In vivo bioluminescence analysis

In vivo lentiviral transduction in brain was monitored by nanoluc bioluminescence imaging using a Xenogen IVIS 200 Imaging System (PerkinElmer). Nano-Glo® In Vivo Substrate from Promega containing the new fluorofurimazine (FFz) was reconstituted by adding 525

μl of 1x sterile PBS to the lyophilized. 100 μl of 2x PBS diluted working solution were intraperitoneal (i.p.) injected in mice. Imaging was acquired 5 min after injection and analysis was performed using Living Image software 4.3.1 (PerkinElmer).

4.12. Mouse tissue preparation for immunofluorescence, bioluminescence and RT-PCR

13 days after lentiviral vector injections or 7 and 14 days after transduced-hNPC injections, mice were intracardially perfused with PBS under Ketamine and Xylazine (i.p.). All organs were collected and stored at −80 °C. For hNPC injected mice, the perfusion was continued with 4% Paraformaldehyde (PFA), brains were removed and stored in 4% PFA for a day and then 30% sucrose solution for 2 days. Mouse brains were coronally sectioned with 16 μm thickness on a freezing cryostat (Leica Microsystems, CM3050S). Lentivirus injected brain sections were alternately collected for immunohistochemistry, bioluminescence and RT-PCR, and hNPC injected brain sections were collected for only immunohistochemistry.

4.13. Immunofluorescence

Lentivirus injected brain sections were post-fixed with 4% PFA for 10 min. Then both lentivirus injected and hNPC injected brain sections were washed with PBS three times and incubated 30 min with blocking solution (PBS/0,1% Triton X-100 containing 10% normal goat serum [Sigma-Aldrich]) and then incubated overnight at 4 °C in blocking solution with primary antibodies: mouse anti-Flag (Sigma, F3165–2 MG, 1:1000); rabbit anti-red fluorescence protein (RFP) (Invitrogen, R10367, 1:1000); rabbit anti-PAX6 (Abcam, ab5790, 1:50); mouse anti-Nestin (Abcam, ab22035, 1:100), rabbit anti-Ki67 (Abcam, ab15580, 1:1000) and mouse anti-human nuclear antigen (Abcam, ab191181, 1:1000). Sections were washed with PBS and incubated for 1 h at room temperature with the secondary antibodies: goat anti-mouse IgG Alexa Fluor 488 (Thermo Fisher, A31560, 1:500); goat anti-rabbit IgG TRITC (Abcam, ab6718, 1:1000) and goat anti-mouse IgG Alexa Fluor 647 (Invitrogen, A32728, 1:1000) diluted in blocking solution. The sections were washed with PBS and mounted with Vectashield Antifade Mounting Medium (Vector Labs, H-1000). Immunofluorescence was visualized and imaged with a Keyence BZ-X810 microscope.

4.14. Bioluminescence assays

Nanoluciferase expression in brain sections, EVs samples and mouse peripheral organs were analyzed with the addition of furimazine (Nano-Glo® Luciferase, Promega) diluted 1:250 in 1X PBS. Samples were incubated with the reagent for at least 1 min prior to reading on Synergy H1 Hybrid Multi-Mode Reader (BioTek). At least 2 reads were performed, and the average value were considered for analysis. For luminescent readings samples were loaded into white 96-well culture plates (Lumitrac 200). Each sample was loaded in duplicate with a volume of ranging from 50 to 100 μl in each well.

4.15. EV isolation from mouse serum via anti-Flag tag magnetic beads

Mouse blood samples were collected into EDTA treated tubes prior and during cardiac PBS perfusions of lentivirus injected and NPC injected mice. Then blood samples were centrifuged at 2000g at room temperature for 10 min. Serum was removed from the

upper layer and incubated with anti-Flagmagnetic beads (Sigma) for 24–48 h at 4 °C on a HulaMixer. Beads containing EVs were pulled down and washed 2x with PBS.

4.16. hNPC isolation from mouse brains via anti-Flag tag magnetic beads

14 days after hNPC engraftments, nude mice were intracardiac perfused with cold PBS. The brains were removed and a 2 mm-thick coronal section containing striatum was cut from every brains. The Neural Tissue Dissociation Kit (Miltenyi Biotec) was used according to manufacturer's instructions to generate single-cell suspensions from these coronal sections. The cell pellets were incubated with anti-Flagmagnetic beads (Sigma) for an hour at room temperature on a HulaMixer. Beads containing hNPCs were pulled down, and washed 2x with PBS.

4.17. RNA extraction, cDNA synthesis and RT-PCR

RNA extraction was performed from the cultured or mouse brain injected NPCs, mouse organs and anti-Flag positive serum EVs following the protocol recommendations of the RNeasy Plus Micro Kit (Qiagen). Isolated RNA samples were quantified by Nanodrop (ThermoFischer Scientific) and Bioanalyzer 2100 (Agilent Technologies, Santa Clara, CA). RNA samples were reverse transcribed using the SuperScript VILO cDNA Synthesis Kit (ThermoFisher Scientific). RT-qPCR was performed using the following primers designed to detect copGFP and Nanoluc mRNA (Primers section).

4.18. Digital droplet PCR (ddPCR)

To evaluate levels of gene expression of copGFP (Forward primer: CCTCGTACTTCTCGATGCGG; Reverse primer: GGCTACGAGAACCCCTTCCT; Taqman probe: TTGGTGTAGCCGCCGTTGTTGATGGCG) and GAPDH [93] in the cells and EVs, gene expression of copGFP and GAPDH was analyzed using ddPCR following PrimePCR ddPCR Gene Expression Probe Assay. Using the manufacturer's protocol droplets were generated with DG8 Cartridge using QX200 droplet generator (Bio-Rad) and PCR performed with thermal cycling conditions via QX200 Droplet Reader and QuantaSoft Software (Bio-Rad) were used to analyze mRNA levels. Normalization was performed based on the sample volume.

4.19. Primers (RT-PCR)

CCTCGTACTTCTCGATGCGG, Forw_copGFP_PP2

GGCTACGAGAACCCCTTCCT, REV_copGFP_PP2

AGAATCTCGGGGTGTCCGTA, Forw_Nanoluc_PP1

GGCCGTCCGAAATAGTCGAT, Rev_Nanoluc_PP1

AAGGATTGTCCTGAGCGGTG, Forw_Nanoluc_PP2

AACACGGCGATGCCTTCATA, Rev_Nanoluc_PP2

GAPDHAGGTCGGTGTGAACGGATTTG, Fwrd mGAPDH

TGTAGACCATGTAGTTGAGGTCA, Rev mGAPDH

Supplementary Material

Refer to Web version on PubMed Central for supplementary material.

Acknowledgements

We want to acknowledge the contribution of Shivangi Shah, Christine A. Vaine for the work with NPCs. Lilian Cruz and Pike-See Cheah for launching and organizing the implantation of NPCs in mouse brains. We thank Dr. Leif Anderson of NanoView Bioscience for generating the single EV data.

Funding

This work was supported by NIH NCI R35 CA232103 and P01 CA069246 to X.O.B., FCT–UID/NEU/04539/2020 and SpreadSilencing POCI-01-0145-FEDER-029716 to L.P.A., SFRH/BD/132618/2017 and FLAD proj. 2021/0001 to D.R.R. We thank Dr. Casey A. Maguire from the Molecular Neurogenetics Unit at MGH for the use of his ExoView R100 device. The MGH Vector Core was supported by NIH NINDS grant P30 NS045776.

Glossary

NoMi	**N**anoluciferase **o**utside and **M**Cherry **i**nside
EVs	Extracellular Vesicles
TSN	Tetraspanin
MVB	Multivesicular Body
ILV	Intraluminal Vesicle
CNS	Central Nervous System
BBB	Blood Brain Barrier
hNPCs	human Neural Progenitor Cells

References

[1]. Raposo Graça, Stoorvogel Willem, Extracellular vesicles: exosomes, microvesicles, and friends, JCB (J. Cell Biol.) 200 (4) (2013) 373–383, 10.1083/jcb.201211138. [PubMed: 23420871]

[2]. Rufino-Ramos David, Albuquerque Patrícia R., Carmona Vitor, Perfeito Rita, Nobre Rui Jorge, de Almeida Luis Pereira, Extracellular vesicles: novel promising delivery systems for therapy of brain diseases, J. Contr. Release 262 (June) (2017) 247–258, 10.1016/j.jconrel.2017.07.001.

[3]. van Niel Guillaume, D'Angelo Gisela, Raposo Graça, Shedding light on the cell biology of extracellular vesicles, Nat. Rev. Mol. Cell Biol 19 (4) (2018) 213–228, 10.1038/nrm.2017.125. [PubMed: 29339798]

[4]. Abels Erik R., Breakefield Xandra O., Introduction to extracellular vesicles: biogenesis, RNA cargo selection, content, release, and uptake, Cell. Mol. Neurobiol 36 (3) (2016) 301–312, 10.1007/s10571-016-0366-z. [PubMed: 27053351]

[5]. Raposo Graça, Stahl Philip D., Extracellular vesicles: a new communication paradigm? Nat. Rev. Mol. Cell Biol 20 (9) (2019) 509–510, 10.1038/s41580-019-0158-7. [PubMed: 31324871]

[6]. Sybren LN Maas, Xandra O. Breakefield, Alissa M. Weaver, Extracellular vesicles: unique intercellular delivery vehicles, Trends Cell Biol 27 (3) (2017) 172–188, 10.1016/j.tcb.2016.11.003. [PubMed: 27979573]

[7]. Mathieu Mathilde, Lorena Martin-Jaular, Lavieu Grégory, Théry Clotilde, Specificities of secretion and uptake of exosomes and other extracellular vesicles for cell-to-cell communication, Nat. Cell Biol 21 (1) (2019) 9–17, 10.1038/s41556-018-0250-9. [PubMed: 30602770]

[8]. Andreu Zoraida, Yáñez-Mó María, Tetraspanins in extracellular vesicle formation and function, Front. Immunol 5 (2014) 442, 10.3389/fimmu.2014.00442. [PubMed: 25278937]

[9]. Théry Clotilde, Witwer Kenneth W., Elena Aikawa, Alcaraz Maria Jose, Anderson Johnathon D., Andriantsitohaina Ramaroson, Anna Antoniou, et al. , Minimal information for studies of extracellular vesicles 2018 (MISEV2018): a position statement of the international society for extracellular vesicles and update of the MISEV2014 guidelines, J. Extracell. Vesicles 7 (1) (2018), 10.1080/20013078.2018.1535750.

[10]. Mathieu Mathilde, Névo Nathalie, Jouve Mabel, Valenzuela José Ignacio, Maurin Mathieu, Verweij Frederik J., Palmulli Roberta, et al. , Specificities of exosome versus small ectosome secretion revealed by live intracellular tracking of CD63 and CD9, Nat. Commun 12 (1) (2021), 10.1038/s41467-021-24384-2.

[11]. Hurwitz Stephanie N., Conlon Meghan M., Rider Mark A., Brownstein Naomi C., Meckes David G. Jr., Nanoparticle analysis sheds budding insights into genetic drivers of extracellular vesicle biogenesis, J. Extracell. Vesicles 5 (2016), 31295, 10.3402/jev.v5.31295. [PubMed: 27421995]

[12]. Corso Giulia, Wolf Heusermann, Trojer Dominic, Görgens André, Steib Emmanuelle, Voshol Johannes, Graff Alexandra, et al. , Systematic characterization of extracellular vesicles sorting domains and quantification at the single molecule–single vesicle level by fluorescence correlation spectroscopy and single particle imaging, J. Extracell. Vesicles 8 (1) (2019), 10.1080/20013078.2019.1663043.

[13]. Hurwitz Stephanie N., Nkosi Dingani, Conlon Meghan M., York Sara B., Liu Xia, Tremblay Deanna C., Meckes David G. Jr., CD63 regulates epstein-barr virus LMP1 exosomal packaging, enhancement of vesicle production, and noncanonical NF-?b signaling, J. Virol 91 (5) (2017), 10.1128/JVI.02251-16.

[14]. Corrigan Laura, Redhai Siamak, Leiblich Aaron, Fan Shih-Jung, Perera Sumeth M. W., Patel Rachel, Gandy Carina, et al. , BMP-regulated exosomes from Drosophila male reproductive glands reprogram female behavior, J. Cell Biol 206 (5) (2014) 671–688, 10.1083/jcb.201401072. [PubMed: 25154396]

[15]. Sandfeld-Paulsen Birgitte, Jakobsen Kristine Raaby, Rikke Bæk, Folkersen Birgitte Holst, Rasmussen Torben Riis, Meldgaard Peter, Kim Varming, Jørgensen Malene Møller, Sorensen Boe Sandahl, Exosomal proteins as diagnostic biomarkers in lung cancer, J. Thorac. Oncol. : Off. Pub. Int. Assoc. Study of Lung Cancer 11 (10) (2016) 1701–1710, 10.1016/j.jtho.2016.05.034.

[16]. Pan Sijun, Zhang Yan, Natalia Auginia, Carine Z, Lim J, Nicholas R, Ho Y, Chowbay Balram, Tze Ping Loh John K., Tam C, Shao Huilin, Extracellular vesicle drug occupancy enables real-time monitoring of targeted cancer therapy, Nat. Nanotechnol 16 (6) (2021) 734–742, 10.1038/s41565-021-00872-w. [PubMed: 33686255]

[17]. Tian Fei, Zhang Shaohua, Liu Chao, Han Ziwei, Liu Yuan, Deng Jinqi, Li Yike, et al. , Protein analysis of extracellular vesicles to monitor and predict therapeutic response in metastatic breast cancer, Nat. Commun 12 (1) (2021) 2536, 10.1038/s41467-021-22913-7. [PubMed: 33953198]

[18]. Skog Johan, Tom Würdinger, van Rijn Sjoerd, Meijer Dimphna H., Gainche Laura, Sena-Esteves Miguel, Curry William T. Jr., Carter Bob S., Krichevsky Anna M., Xandra O. Breakefield, Glioblastoma microvesicles transport RNA and proteins that promote tumour growth and provide diagnostic biomarkers, Nat. Cell Biol 10 (12) (2008) 1470–1476, 10.1038/ncb1800. [PubMed: 19011622]

[19]. Shao Huilin, Chung Jaehoon, Balaj Leonora, Charest Alain, Bigner Darell D., Carter Bob S., Hochberg Fred H., Breakefield Xandra O., Weissleder Ralph, Lee Hakho, Protein typing of circulating microvesicles allows real-time monitoring of glioblastoma therapy, Nat. Med 18 (12) (2012) 1835–1840, 10.1038/nm.2994. [PubMed: 23142818]

[20]. Chi Andrew S., Cahill Daniel P., Reardon David A., Wen Patrick Y., Mikkelsen Tom, Peereboom David M., Wong Eric T., et al. , Exploring predictors of response to dacomitinib in EGFR-amplified recurrent glioblastoma, JCO Precision Oncology 4 (2020), 10.1200/PO.19.00295.

[21]. Ricklefs Franz L., Alayo Quazim, Krenzlin Harald, Mahmoud Ahmad B., Speranza Maria C., Nakashima Hiroshi, Hayes Josie L., et al. , Immune evasion mediated by PD-L1 on glioblastoma-derived extracellular vesicles, Sci. Adv 4 (3) (2018) eaar2766, 10.1126/sciadv.aar2766.

[22]. Ramirez Servio H., Andrews Allison M., Paul Debayon, Pachter Joel S., Extracellular vesicles: mediators and biomarkers of pathology along CNS barriers, in: Fluids And Barriers Of the CNS, BioMed Central Ltd, 2018, 10.1186/s12987-018-0104-7.

[23]. Zhang Jingjing, Nguyen Luong T.H., Hickey Richard, Walters Nicole, Wang Xinyu, Kwak Kwang Joo, Lee L James, Palmer Andre F., Reátegui Eduardo, Immunomagnetic sequential ultrafiltration (ISUF) platform for enrichment and purification of extracellular vesicles from biofluids, Sci. Rep 11 (1) (2021) 8034, 10.1038/s41598-021-86910-y. [PubMed: 33850163]

[24]. Fowler Christie D., NeuroEVs: characterizing extracellular vesicles generated in the neural domain, J. Neurosci 39 (47) (2019) 9262–9268, 10.1523/JNEUROSCI.0146-18.2019. [PubMed: 31748281]

[25]. Cheng Lesley, Vella Laura J., Barnham Kevin J., McLean Catriona, Masters Colin L., Hill Andrew F., Small RNA fingerprinting of Alzheimer's disease frontal cortex extracellular vesiclesand their comparison with peripheral extracellular vesicles, J. Extracell. Vesicles 9 (1) (2020), 10.1080/20013078.2020.1766822.

[26]. Hill Andrew F., Fowler Christie D., Dual perspectives dual perspectives companion paper: extracellular vesicles and neurodegenerative diseases, NeuroEVs: Characterizing Extracellular Vesicles Generated in the Neural Domain 39 (47) (2019) 9269–9273, 10.1523/JNEUROSCI.0146-18.2019.

[27]. Thompson Alexander G., Gray Elizabeth, Heman-Ackah Sabrina M., Mäger Imre, Talbot Kevin, El Andaloussi Samir, Wood Matthew J., Turner Martin R., Extracellular vesicles in neurodegenerative disease — pathogenesis to biomarkers, Nat. Rev. Neurol 12 (6) (2016) 346–357, 10.1038/nrneurol.2016.68. [PubMed: 27174238]

[28]. Hill Andrew F., NeuroEVs : characterizing extracellular vesicles generated in the neural domain, by extracellular vesicles and neurodegenerative diseases, J. Neurosci 39 (47) (2019) 9269–9273. [PubMed: 31748282]

[29]. Lu Yunhe, Chen Lei, Li Liangdong, Cao Yiqun, Exosomes derived from brain metastatic breast cancer cells destroy the blood-brain barrier by carrying LncRNA GS1–600g8.5, BioMed Res. Int 2020 (2020), 10.1155/2020/7461727.

[30]. Tominaga Naoomi, Kosaka Nobuyoshi, Ono Makiko, Katsuda Takeshi, Yoshioka Yusuke, Tamura Kenji, Jan Lötvall, Nakagama Hitoshi, Ochiya Takahiro, Brain metastatic cancer cells release MicroRNA-181c-containing extracellular vesicles capable of destructing blood-brain barrier, Nat. Commun 6 (2015), 10.1038/ncomms7716.

[31]. Sharma Pranav, Mesci Pinar, Carromeu Cassiano, McClatchy Daniel R., Schiapparelli Lucio, Yates John R., Muotri Alysson R., Cline Hollis T., Exosomes regulate neurogenesis and circuit assembly, Proc. Natl. Acad. Sci. U. S. A 116 (32) (2019) 16086–16094, 10.1073/pnas.1902513116. [PubMed: 31320591]

[32]. Mahjoum Shadi, Rufino-ramos David, Broekman Marike L.D., Living Proof of Activity of Extracellular Vesicles in the Central Nervous System, 2021.

[33]. Sinha Sardar, Maitrayee Anna Ansell-Schultz, Civitelli Livia, Hildesjö Camilla, Larsson Max, Lannfelt Lars, Martin Ingelsson, Hallbeck Martin, Alzheimer's disease pathology propagation by exosomes containing toxic amyloid-beta oligomers, Acta Neuropathol 136 (1) (2018) 41–56, 10.1007/s00401-018-1868-1. [PubMed: 29934873]

[34]. Polanco Juan Carlos, Scicluna Benjamin James, Hill Andrew Francis, Götz Jürgen, Extracellular vesicles isolated from the brains of RTg4510 mice seed tau protein aggregation in a threshold-dependent manner, J. Biol. Chem 291 (24) (2016) 12445–12466, 10.1074/jbc.M115.709485. [PubMed: 27030011]

[35]. Zappulli Valentina, Friis Kristina Pagh, Fitzpatrick Zachary, Maguire Casey A., Breakefield Xandra O., Extracellular vesicles and intercellular communication within the nervous system, J. Clin. Invest 126 (4) (2016) 1198–1207, 10.1172/JCI81134. [PubMed: 27035811]

[36]. Fowler Christie D., Hill Andrew F., Extracellular Vesicles and Neurodegenerative Diseases, vol. 39, 2019, pp. 9269–9273, 47.

[37]. Norman Maia, Ter-Ovanesyan Dmitry, Trieu Wendy, Lazarovits Roey, Emma J K Kowal, Hyun Lee Ju, Chen-Plotkin Alice S., Regev Aviv, Church George M., Walt David R., L1CAM is not associated with extracellular vesicles in human cerebrospinal fluid or plasma, bioRxiv (2020), 10.1101/2020.08.12.247833, 2020.08.12.247833.

[38]. Shi Min, Sheng Lifu, Stewart Tessandra, Zabetian Cyrus P., Zhang Jing, New windows into the brain: central nervous system-derived extracellular vesicles in blood, July 2018, Prog. Neurobiol 175 (2019) 96–106, 10.1016/j.pneurobio.2019.01.005. [PubMed: 30685501]

[39]. Dmitry Ter-Ovanesyan, Norman Maia, Lazarovits Roey, Trieu Wendy, Lee Ju-Hyun, Church George M., Walt David R., Framework for rapid comparison of extracellular vesicle isolation methods, Elife 10 (2021) 1–17, 10.7554/elife.70725.

[40]. Norman Maia, Ter-Ovanesyan Dmitry, Trieu Wendy, Lazarovits Roey, Kowal Emma J. K., Lee Ju Hyun, Alice S, Chen-Plotkin, Regev Aviv, Church George M., Walt David R., L1CAM is not associated with extracellular vesicles in human cerebrospinal fluid or plasma, Nat. Methods 18 (6) (2021) 631–634, 10.1038/s41592-021-01174-8. [PubMed: 34092791]

[41]. Tkach Mercedes, Kowal Joanna, Théry Clotilde, Why the need and how to approach the functional diversity of extracellular vesicles, Phil. Trans. Biol. Sci 373 (1737) (2018), 10.1098/rstb.2016.0479.

[42]. Daaboul G. George, Gagni Paola, Benussi Luisa, Bettotti Paolo, Ciani Miriam, Cretich Marina, Freedman David S., et al. , Digital detection of exosomes by interferometric imaging, Sci. Rep 6 (1) (2016) 37246, 10.1038/srep37246. [PubMed: 27853258]

[43]. Bachurski Daniel, Schuldner Maximiliane, Nguyen Phuong-Hien, Malz Alexandra, Reiners Katrin S., Grenzi Patricia C., Babatz Felix, et al. , Extracellular vesicle measurements with nanoparticle tracking analysis – an accuracy and repeatability comparison between NanoSight NS300 and ZetaView, J. Extracell. Vesicles 8 (1) (2019), 1596016, 10.1080/20013078.2019.1596016. [PubMed: 30988894]

[44]. Gandham Srujan, Su Xianyi, Wood Jacqueline, Nocera Angela L., Alli Sarath Chandra, Milane Lara, Zimmerman Alan, Amiji Mansoor, Ivanov Alexander R., Technologies and standardization in research on extracellular vesicles, Trends Biotechnol 38 (10) (2020) 1066–1098, 10.1016/j.tibtech.2020.05.012. [PubMed: 32564882]

[45]. O'Brien Killian, Breyne Koen, Ughetto Stefano, Laurent Louise C., Breakefield Xandra O., RNA delivery by extracellular vesicles in mammalian cells and its applications, Nat. Rev. Mol. Cell Biol 21 (10) (2020) 585–606, 10.1038/s41580-020-0251-y. [PubMed: 32457507]

[46]. Wu Anthony Yan Tang, Sung Yun Chieh, Chen Yen Ju, Chou Steven Ting Yu, Guo Vanessa, Chien Jasper Che Yung, Ko John Jun Sheng, et al. , Multiresolution imaging using bioluminescence resonance energy transfer identifies distinct biodistribution profiles of extracellular vesicles and exomeres with redirected tropism, Adv. Sci 7 (19) (2020) 1–17, 10.1002/advs.202001467.

[47]. Luo Weijia, Yuan Dai, Chen Zhishi, Yue Xiaojing, Andrade-Powell C. Kelsey, Jiang Chang, Spatial and temporal tracking of cardiac exosomes in mouse using a nano-luciferase-CD63 fusion protein, Commun. Biol 3 (1) (2020) 1–9, 10.1038/s42003-020-0830-7. [PubMed: 31925316]

[48]. Neradil Jakub, Veselska Renata, Nestin as a marker of cancer stem cells, Cancer Sci 106 (7) (2015) 803–811, 10.1111/cas.12691. [PubMed: 25940879]

[49]. Suter David M., Tirefort Diderik, Julien Stephanie, Krause Karl-Heinz, A Sox1 to Pax6 switch drives neuroectoderm to radial glia progression during differentiation of mouse embryonic stem cells, Stem Cell 27 (1) (2009) 49–58, 10.1634/stemcells.2008-0319.

[50]. Kowal Joanna, Arras Guillaume, Colombo Marina, Jouve Mabel, Morath Jakob Paul, Primdal-Bengtson Bjarke, Dingli Florent, Loew Damarys, Tkach Mercedes, Clotilde Théry, Proteomic comparison defines novel markers to characterize heterogeneous populations of extracellular vesicle subtypes, Proc. Natl. Acad. Sci. U. S. A 113 (8) (2016) E968–E977, 10.1073/pnas.1521230113. [PubMed: 26858453]

[51]. Gupta Dhanu, Liang Xiuming, Pavlova Svetlana, Oscar P, Wiklander B, Corso Giulia, Zhao Ying, Saher Osama, et al. , Quantification of extracellular vesicles in vitro and in vivo using sensitive bioluminescence imaging, J. Extracell. Vesicles 9 (1) (2020), 10.1080/20013078.2020.1800222.

[52]. Gupta Dhanu, Wiklander Oscar, Görgens André, Conceição Mariana, Corso Giulia, Liang Xiuming, Seow Yiqi, et al., Engineering of Extracellular Vesicles for Display of Protein Biotherapeutics, 2020, p. 1, 10.1101/2020.06.14.149823.

[53]. Görgens André, Bremer Michel, Ferrer-Tur Rita, Murke Florian, Tobias Tertel, Horn Peter A., Thalmann Sebastian, et al. , Optimisation of imaging flow cytometry for the analysis of single extracellular vesicles by using fluorescence-tagged vesicles as biological reference material, J. Extracell. Vesicles 8 (1) (2019), 1587567, 10.1080/20013078.2019.1587567. [PubMed: 30949308]

[54]. Gerlach Jared Q., Griffin Matthew D., Getting to know the extracellular vesicle glycome, Mol. Biosyst 12 (4) (2016) 1071–1081, 10.1039/c5mb00835b. [PubMed: 26888195]

[55]. Stipp Christopher S., Kolesnikova Tatiana V., Hemler Martin E., Functional domains in tetraspanin proteins, Trends Biochem. Sci 28 (2) (2003) 106–112, 10.1016/S0968-0004(02)00014-2. [PubMed: 12575999]

[56]. Lozano-Andrés Estefanía, Libregts Sten F., Toribio Victor, Royo Félix, Morales Sara, López-Martín Soraya, Valés-Gómez Mar, et al. , Tetraspanin-decorated extracellular vesicle-mimetics as a novel adaptable reference material, J. Extracell. Vesicles 8 (1) (2019), 10.1080/20013078.2019.1573052.

[57]. Kojima Ryosuke, Bojar Daniel, Rizzi Giorgio, Charpin-el Hamri Ghislaine, El-baba Marie Daoud, Saxena Pratik, Simon Ausländer, Tan Kelly R., Fussenegger Martin, Parkinson ‘ S Disease Treatment, 2018, 10.1038/s41467-018-03733-8.

[58]. Kojima Ryosuke, Bojar Daniel, Rizzi Giorgio, El Hamri Ghislaine Charpin, El-Baba Marie Daoud, Saxena Pratik, Simon Ausländer, Tan Kelly R., Fussenegger Martin, Designer exosomes produced by implanted cells intracerebrally deliver therapeutic cargo for Parkinson’s disease treatment, Nat. Commun 9 (1) (2018), 10.1038/s41467-018-03733-8.

[59]. Zijlstra Andries, Dolores Di Vizio, Size matters in nanoscale communication, Nat. Cell Biol 20 (3) (2018) 228–230, 10.1038/s41556-018-0049-8. [PubMed: 29476154]

[60]. Gerace Erica, Moazed Danesh, Affinity pull-down of proteins using anti-FLAG M2 agarose beads, Methods Enzymol 559 (2015) 99–110, 10.1016/bs.mie.2014.11.010. [PubMed: 26096505]

[61]. Sakakura Hiroki, Mii Shinji, Hagiwara Sumitaka, Kato Takuya, Yamamoto Noriyuki, Hibi Hideharu, Takahashi Masahide, Murakumo Yoshiki, CD109 is a component of exosome secreted from cultured cells, Biochem. Biophys. Res. Commun 469 (4) (2016) 816–822, 10.1016/j.bbrc.2015.12.063. [PubMed: 26707640]

[62]. He Hongjian, Wang Jiaqing, Wang Huaimin, Zhou Ning, Yang Dongsik, Green Douglas R., Xu Bing, Enzymatic cleavage of branched peptides for targeting mitochondria, J. Am. Chem. Soc 140 (4) (2018) 1215–1218, 10.1021/jacs.7b11582. [PubMed: 29328651]

[63]. Zaborowski Mikołaj Piotr, Cheah Pike See, Zhang Xuan, Bushko Isabella, Lee Kyungheon, Sammarco Alessandro, Zappulli Valentina, et al. , Membrane-bound Gaussia luciferase as a tool to track shedding of membrane proteins from the surface of extracellular vesicles, Sci. Rep 9 (1) (2019) 17387, 10.1038/s41598-019-53554-y. [PubMed: 31758005]

[64]. Wilmann Pascal G., Battad Jion, Petersen Jan, Wilce Matthew C.J., Dove Sophie, Devenish Rodney J., Prescott Mark, Rossjohn Jamie, The 2.1A crystal structure of CopGFP, a representative member of the copepod clade within the green fluorescent protein superfamily, J. Mol. Biol 359 (4) (2006) 890–900, 10.1016/j.jmb.2006.04.002. [PubMed: 16697009]

[65]. Chudakov Dmitriy M., Matz Mikhail V., Lukyanov Sergey, Lukyanov Konstantin A., Fluorescent Proteins and Their Applications in Imaging Living Cells and Tissues, 2021, 10.1152/physrev.00038.2009, 1103–63.

[66]. Evdokimov Artem G., Pokross Matthew E., Egorov Nikolay S., Zaraisky Andrey G., Yampolsky Ilya V., Merzlyak Ekaterina M., Shkoporov Andrey N., Sander Ian, Lukyanov Konstantin A., Chudakov Dmitriy M., Structural basis for the fast maturation of arthropoda green fluorescent protein, EMBO Rep 7 (10) (2006) 1006–1012, 10.1038/sj.embor.7400787. [PubMed: 16936637]

[67]. Stepanenko Olga V., Sulatsky Maksim I., Mikhailova Ekaterina V., Kuznetsova Irina M., Turoverov Konstantin K., Olesya V Stepanenko, Sulatskaya Anna I., New findings on GFP-like protein application as fluorescent tags: fibrillogenesis, oligomerization, and amorphous aggregation, Int. J. Biol. Macromol 192 (2021) 1304–1310, 10.1016/j.ijbiomac.2021.10.107. [PubMed: 34687761]

[68]. Sung Bong Hwan, von Lersner Ariana, Guerrero Jorge, Krystofiak Evan S., Inman David, Pelletier Roxanne, Zijlstra Andries, Ponik Suzanne M., Weaver Alissa M., A live cell reporter of exosome secretion and uptake reveals pathfinding behavior of migrating cells, Nat. Commun 11 (1) (2020) 2092, 10.1038/s41467-020-15747-2. [PubMed: 32350252]

[69]. Goetzl Edward J., Adam Boxer Janice B., Schwartz Erin L., Abner Ronald C., Miller Petersen Bruce L., Kapogiannis Dimitrios, Altered lysosomal proteins in neural-derived plasma exosomes in preclinical alzheimer disease, Neurology 85 (1) (2015) 40–47, 10.1212/WNL.0000000000001702. [PubMed: 26062630]

[70]. Mustapic Maja, Eitan Erez, Werner John K., Berkowitz Sean T., Lazaropoulos Michael P., Tran Joyce, Goetzl Edward J., Kapogiannis Dimitrios, Plasma extracellular vesicles enriched for neuronal origin: a potential window into brain pathologic processes, Front. Neurosci 11 (MAY) (2017) 1–12, 10.3389/fnins.2017.00278. [PubMed: 28154520]

[71]. Linares Romain, Tan Sisareuth, Gounou Céline, Brisson Alain R., Imaging and quantification of extracellular vesicles by transmission electron microscopy, Methods Mol. Biol 1545 (2017) 43–54, 10.1007/978-1-4939-6728-5_4. [PubMed: 27943206]

[72]. Brisson Alain R., Tan Sisareuth, Linares Romain, Gounou Céline, Arraud Nicolas, Extracellular vesicles from activated platelets: a semiquantitative cryo-electron microscopy and immuno-gold labeling study, Platelets 28 (3) (2017) 263–271, 10.1080/09537104.2016.1268255. [PubMed: 28102751]

[73]. Lai Charles P., Mardini Osama, Ericsson Maria, Prabhakar Shilpa, Maguire Casey, Chen John W., Tannous Bakhos A., Breakefield Xandra O., Dynamic biodistribution of extracellular vesicles in vivo using a multimodal imaging reporter, ACS Nano 8 (1) (2014) 483–494, 10.1021/nn404945r. [PubMed: 24383518]

[74]. Lai Charles P., Kim Edward Y., Badr Christian E., Weissleder Ralph, Mempel Thorsten R., Tannous Bakhos A., Breakefield Xandra O., Visualization and tracking of tumour extracellular vesicle delivery and RNA translation using multiplexed reporters, Nat. Commun 6 (May) (2015) 1–12, 10.1038/ncomms8029.

[75]. Verweij Frederik J., Balaj Leonora, Boulanger Chantal M., Carter David R.F., Compeer Ewoud B., D'Angelo Gisela, El Andaloussi Samir, et al. , The power of imaging to understand extracellular vesicle biology in vivo, Nat. Methods 18 (9) (2021) 1013–1026, 10.1038/s41592-021-01206-3. [PubMed: 34446922]

[76]. Bebelman Maarten P., Philippe Bun, Huveneers Stephan, van Niel Guillaume, Pegtel D Michiel, Verweij Frederik J., Real-time imaging of multivesicular body–plasma membrane fusion to quantify exosome release from single cells, Nat. Protoc 15 (1) (2020) 102–121, 10.1038/s41596-019-0245-4. [PubMed: 31836866]

[77]. Wei Zhiyun, Batagov Arsen O., Schinelli Sergio, Wang Jintu, Wang Yang, El Fatimy Rachid, Rabinovsky Rosalia, et al. , Coding and noncoding landscape of extracellular RNA released by human glioma stem cells, Nat. Commun 8 (1) (2017) 1145, 10.1038/s41467-017-01196-x. [PubMed: 29074968]

[78]. Shagin Dmitry A., Barsova Ekaterina V., Yanushevich Yurii G., Fradkov Arkady F., Lukyanov Konstantin A., Labas Yulii A., Semenova Tatiana N., et al. , GFP-like proteins as ubiquitous metazoan superfamily: evolution of functional features and structural complexity, Mol. Biol. Evol 21 (5) (2004) 841–850, 10.1093/molbev/msh079. [PubMed: 14963095]

[79]. Tannous Bakhos A., Gaussia luciferase reporter assay for monitoring biological processes in culture and in vivo, Nat. Protoc 4 (4) (2009) 582–591, 10.1038/nprot.2009.28. [PubMed: 19373229]

[80]. Charles Joël P., Fuchs Jeannette, Hefter Mirjam, Vischedyk Jonas B., Kleint Maximilian, Vogiatzi Fotini, Schäfer Jonas A., et al. , Monitoring the dynamics of clonal tumour evolution in vivo using secreted luciferases, Nat. Commun 5 (June) (2014) 3981, 10.1038/ncomms4981. [PubMed: 24889111]

[81]. Hall Mary P., Unch James, Binkowski Brock F., Valley Michael P., Butler Braeden L., Wood Monika G., Otto Paul, et al. , Engineered luciferase reporter from a deep sea shrimp utilizing a novel imidazopyrazinone substrate, ACS Chem. Biol 7 (11) (2012) 1848–1857, 10.1021/cb3002478. [PubMed: 22894855]

[82]. Su Yichi, Walker Joel R., Park Yunhee, Smith Thomas P., Liu Lan Xiang, Hall Mary P., Labanieh Louai, et al. , Novel NanoLuc substrates enable bright two-population bioluminescence imaging in animals, Nat. Methods 17 (8) (2020) 852–860, 10.1038/s41592-020-0889-6. [PubMed: 32661427]

[83]. Blits Bas, Derks Sanne, Twisk Jaap, Ehlert Erich, Prins Jolanda, Verhaagen Joost, Adeno-associated viral vector (AAV)-Mediated gene transfer in the red nucleus of the adult rat brain: comparative analysis of the transduction properties of seven AAV serotypes and lentiviral vectors, J. Neurosci. Methods 185 (2) (2010) 257–263, 10.1016/j.jneumeth.2009.10.009. [PubMed: 19850079]

[84]. Cearley Cassia N., Wolfe John H., A single injection of an adeno-associated virus vector into nuclei with divergent connections results in widespread vector distribution in the brain and global correction of a neurogenetic disease, J. Neurosci. : Off. J. Soc. Neurosci 27 (37) (2007) 9928–9940, 10.1523/JNEUROSCI.2185-07.2007.

[85]. Dautzenberg Iris J.C., Rabelink Martijn J.W.E., Hoeben Rob C., The stability of envelope-pseudotyped lentiviral vectors, Gene Ther 28 (1–2) (2021) 89–104, 10.1038/s41434-020-00193-y. [PubMed: 32973351]

[86]. Men Yuqin, Yelick Julia, Jin Shijie, Tian Yang, Chiang Ming Sum R., Higashimori Haruki, Brown Eoin, Jarvis Rachel, Yang Yongjie, Exosome reporter mice reveal the involvement of exosomes in mediating neuron to astroglia communication in the CNS, Nat. Commun 10 (1) (2019), 10.1038/s41467-019-11534-w.

[87]. Odeberg J, Wolmer N, Falci S, Westgren M, Seiger Å, Söderberg-Nauclér C, Human cytomegalovirus inhibits neuronal differentiation and induces apoptosis in human neural precursor cells, J. Virol 80 (2006) 8929–8939. [PubMed: 16940505]

[88]. Mendonça Liliana S., Nóbrega Clévio, Hirai Hirokazu, Kaspar Brian K., De Almeida Lu Pereira, Transplantation of cerebellar neural stem cells improves motor coordination and neuropathology in machado-joseph disease mice, Brain 138 (2) (2015) 320–335, 10.1093/brain/awu352. [PubMed: 25527827]

[89]. Cossetti Chiara, Iraci Nunzio, Mercer Tim R., Leonardi Tommaso, Alpi Emanuele, Drago Denise, Alfaro-Cervello Clara, et al. , Extracellular vesicles from neural stem cells transfer IFN-γ via Ifngr1 to activate Stat1 signaling in target cells, Mol. Cell 56 (2) (2014) 193–204, 10.1016/j.molcel.2014.08.020. [PubMed: 25242146]

[90]. Bian Baishijiao, Zhao Congjian, He Xiangyu, Gong Yu, Ren Chunge, Ge Lingling, Zeng Yuxiao, et al. , Exosomes derived from neural progenitor cells preserve photoreceptors during retinal degeneration by inactivating microglia, J. Extracell. Vesicles 9 (1) (2020), 10.1080/20013078.2020.1748931.

[91]. Webb Robin L., Kaiser Erin E., Scoville Shelley L., Thompson Tyler A., Fatima Sumbul, Pandya Chirayukumar, Sriram Karishma, et al. , Human neural stem cell extracellular vesicles improve tissue and functional recovery in the murine thromboembolic stroke model, Trans. Stroke Res 9 (5) (2018) 530–539, 10.1007/s12975-017-0599-2.

[92]. de D Zala Almeida LP, Aebischer P, Déglon N, Neuroprotective effect of a CNTF-expressing lentiviral vector in the quinolinic acid rat model of huntington's disease, Neurobiol. Dis 8 (3) (2001) 433–446, 10.1006/nbdi.2001.0388. [PubMed: 11442352]

[93]. Ali Jamal Al, Vaine Christine A., Shah Shivangi, Campion Lindsey, Ahmad Hakoum, Supnet Melanie L., Acuña Patrick, et al. , TAF1 transcripts and neurofilament light chain as biomarkers for X-linked dystonia-parkinsonism, Mov. Disord. : Off. J. Movement Dis. Soc 36 (1) (2021) 206–215, 10.1002/mds.28305.

[94]. Carmona Vitor, Cunha-Santos Janete, Onofre Isabel, Simões Ana Teresa, Vijayakumar Udaya, Davidson Beverly L., Luís Pereira de Almeida, Unravelling endogenous MicroRNA system dysfunction as a new pathophysiological mechanism in machado-joseph disease, Mol. Ther 25 (4) (2017) 1038–1055, 10.1016/j.ymthe.2017.01.021. [PubMed: 28236575]

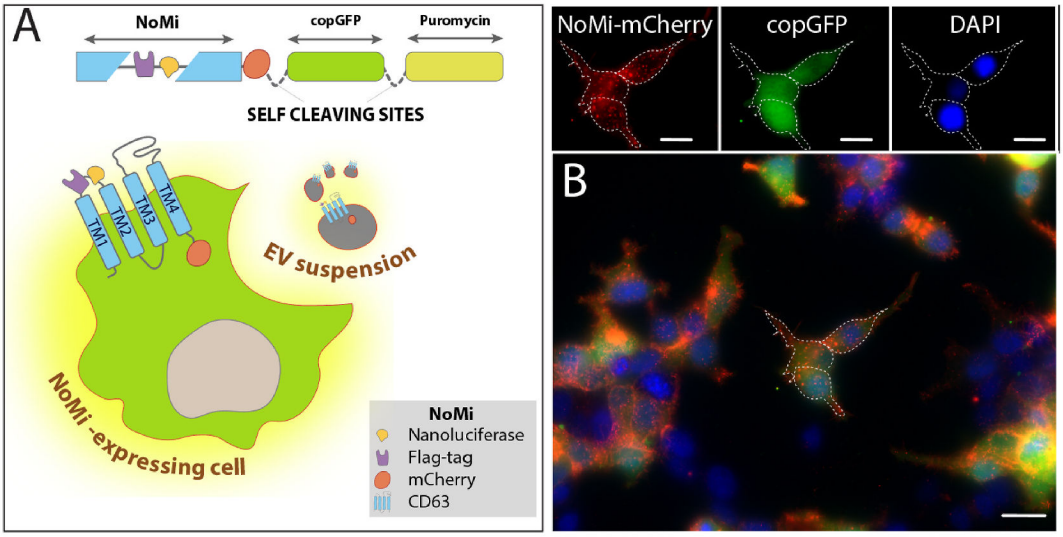

Fig. 1. NoMi tracer expressed in cells.

(A) Cartoon explaining NoMi (**N**anoluc **o**utside and **m**Cherry **i**nside) design to detect EVs secreted into cell media. NoMi uses CD63 as a scaffold to connect the exposed surface (Flag tag and nanoluciferase) with the inner surface (mCherry) of the cell or EVs. TM = transmembrane domain. (B) HEK293T cells expressing the NoMi construct with green fluorescence (copGFP) expressed in cytoplasm and red fluorescence (mCherry) expressed in NoMi-EV generating membrane compartments within the cells. Scale bar represents 20 μm. (For interpretation of the references to colour in this figure legend, the reader is referred to the Web version of this article.)

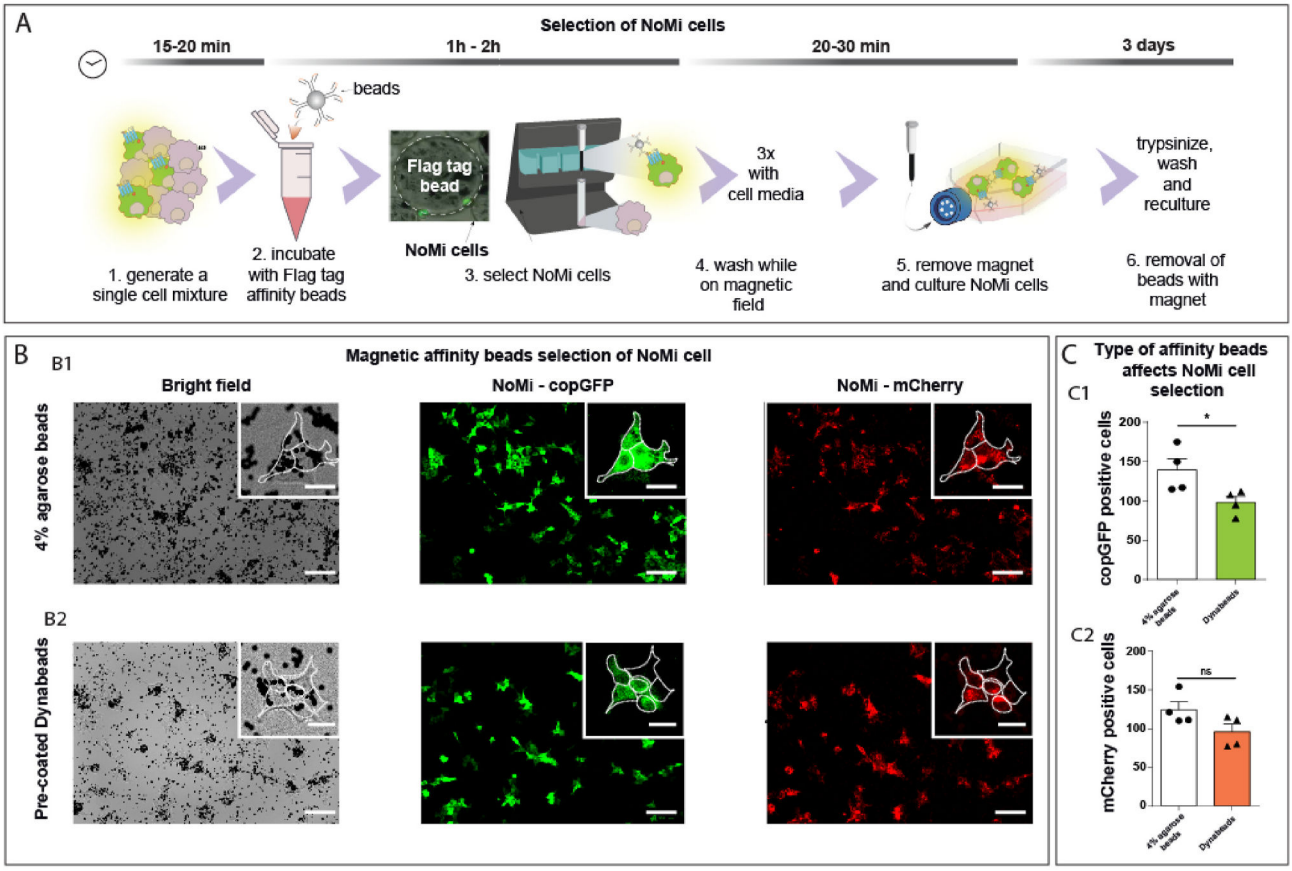

Fig. 2. Cell-selection with Flag tagged NoMi-construct.

(A) Schematic representation of NoMi operation to isolate NoMi-expressing cells. A Flag tag on the outer surface of the cells can be used to select transduced NoMi-cells from cell mixture through antibody based magnetic bead affinity selection. A NoMi-containing single cell suspension is incubated with Flag tag affinity beads, whereby NoMi-cells get captured from the cell mixture by their Flag tag on the cell surface. After washing off non-NoMi expressing cells, bead-bound NoMi cells are cultured in a culturing flask. Following three days of culturing, cells are trypsinized and exposed to a magnet to ensure bead removal from the NoMi cells in the next culturing step. (B) Flag tag affinity bead composition dictates efficiency of NoMi expressing HEK293T cell capture. Representative fluorescent microscopy images of bead-captured NoMi cells at step 5 of the NoMi operation with anti-Flag M2 magnetic beads that are 4% agarose beads [B1] and Flag antibody pre-coated Dynabeads [B2]. (C) The type of magnetic beads affects NoMi-cell selection. [C1] Quantification of copGFP fluorescence shows significantly more cells captured by anti-Flag M2 magnetic beads that are 4% agarose beads when compared to Flag antibody pre-coated Dynabeads. [C2] A similar tendency was verified upon mCherry fluorescence analysis. Data represents four replicates and are presented as mean with SEM (error bars) and *p < 0.01 Unpaired *t*-test. Scale bar is 100 μm in low and 25 μm in high magnification.

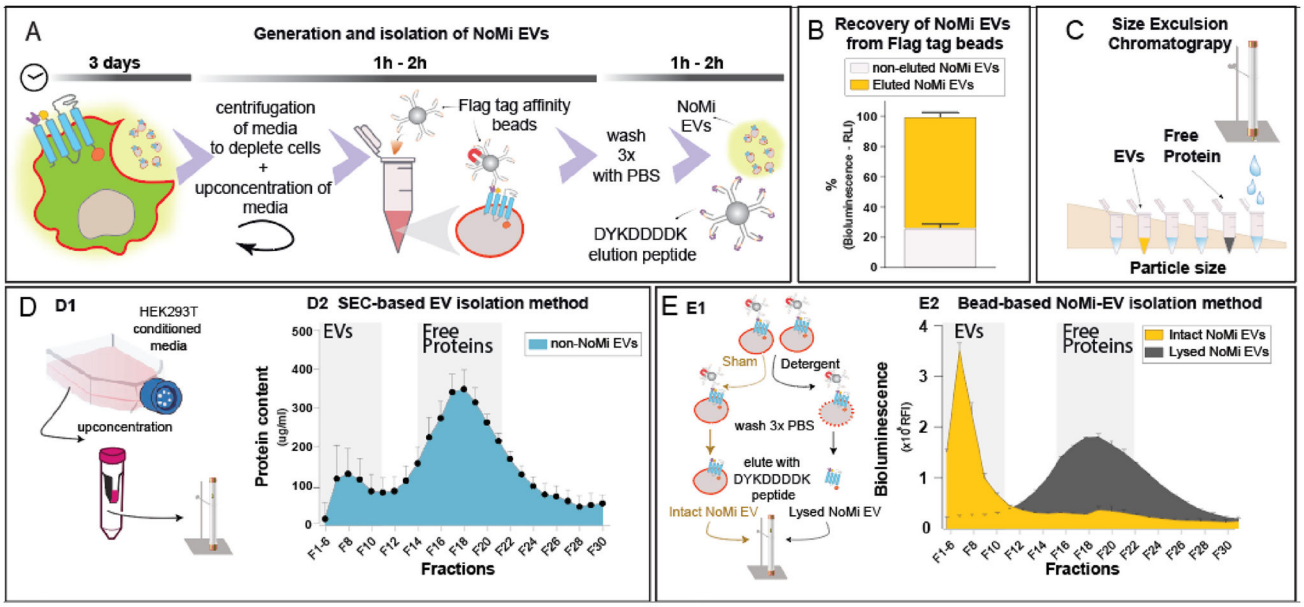

Fig. 3. NoMi construct enables EV purification from complex biofluids.

(A) NoMi operation to isolate NoMi-expressing EVs. NoMi construct expressing HEK293T cells expose a Flag tag to the outer surface, a characteristic adopted by their NoMi-EV progeny. This affinity tag can be used to isolate NoMi-EVs. We collected the conditioned media after 3 days of culturing NoMi-cells, depleted the cells by centrifugation and concentrated the media with a 100 kDa cut-off filter. After incubation of Flag tag affinity beads, NoMi-EVs get captured from the concentrated media by their Flag tag exposure. The bead bound NoMi-EVs are washed to eliminate non-NoMi-EV constituents when the suspension is under a magnetic field. Elution with a Flag tag (DYDKDDDK) peptide ensures elution of NoMi-EVs and generates a dense NoMi-EV suspension. The beads are removed from the NoMi-EV suspension by a magnet. (B) Elution of EVs with Flag tag peptide enables recovery of 75% of EVs from the magnetic beads determined with bioluminescent nanoluciferase signal in NoMi (n = 4). (C) Schematic of how EVs can be characterized based on their particle size with size exclusion chromatography (SEC). Big particles, including EVs, elute first while smaller particles such as proteins elute later. This method can be used to verify the presence of contaminating protein in EV suspensions. (D) EV isolation of non-NoMi-EVs. [D1] Schematic of how conditioned media of HEK293T cells was concentrated with a 100 kDa cut-off filter and resolved on a SEC column before being characterized based on protein content. [D2] The predominant SEC peak was observed in the free protein fractions, while little signal was detected in the fractions in the particle size range where we expect to retrieve EVs. This measurement was performed with a protein assay and demonstrates the difficulty in resolving EVs from free protein. (n = 3) (E) NoMi-EVs isolated with the NoMi operation were resolved on a SEC column. [E1] Schematic representation shows that prior to elution, bead captured NoMi-EV were either detergent (n = 2) or sham (n = 2) treated prior to washing with PBS and elution with Flag tag peptide. [E2] When SEC-resolved, sham treated intact NoMi-EVs were predominantly retrieved in the early EV particle size range fractions, while the detergent treated and lysed NoMi-EVs were found in the later free protein size range fractions. Detection of our

NoMi-construct was performed with NoMi-Nanoluc bioluminescence. Data are presented as mean with SEM (error bars).

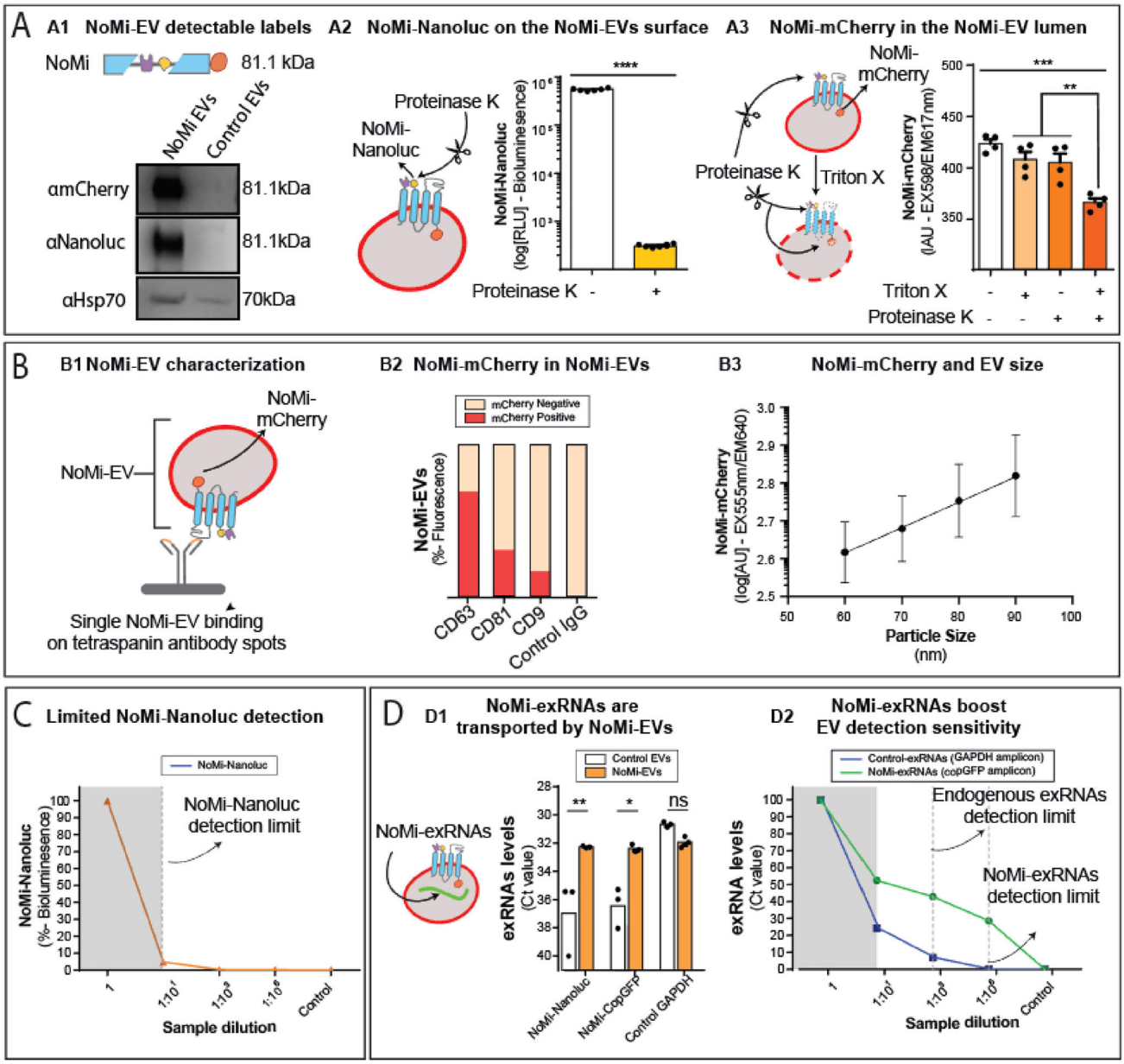

Fig. 4. Characterization of NoMi-EVs in crude SEC-resolved EV samples.

(A) Bulk EVs characterization of NoMi-labels. [A1] The size of our NoMi-construct is 81.1 kDa. Western blots show Nanoluc, mCherry and Hsp70 in NoMi-EVs and HEK293T EV control sample. [A2] EV surface exposed NoMi-Nanoluc is degraded upon treatment with Proteinase K. Data measured with NoMi-bioluminescence (N = 6). [A3] EV lumen exposed NoMi-mCherry fluorescent signal post-proteinase K degradation of NoMi-EVs with and without detergent (Triton X) treatment (N = 4). (B) Single NoMi-EV characterization. [B1] Representation of the Exoview method to immobilize NoMi-EVs for single EV characterization. [B2] NoMi-EVs isolated from cell media by SEC can be distinguished from other non-NoMi EVs based on NoMi-mCherry fluorescence observed post-antibody capture of CD63 (69%), CD81 (30%), and CD9 (16.5%) tetraspanins. [B3] Tendency for

a correlation between particle size and NoMi-mCherry fluorescence ranging from 60 to 90 nm in particle size. (C) The number of NoMi-labels per NoMi-EV limits their detection in samples. Data shown with NoMi-Nanoluc bioluminescence (N = 3). (D) NoMi-exRNAs are transported within NoMi-EVs. [D1] NoMi-exRNAs can be detected by PCR, including CopGFP and Nanoluc exRNAs. These are significantly increased compared to non-NoMi HEK293T EVs in contrast to endogenous exRNAs, such as GAPDH (N = 3). [D2] CopGFP-exRNAs are 1000x more abundant than GAPDH-exRNA in NoMi-EVs, boosting detection when addressing small numbers of EVs (N = 3). Data represent at least three experiments and are presented as the mean with SEM (error bars). One-way ANOVA with Tukey's multiple-comparisons test. *$p < 0.05$, **$p < 0.01$, ***$p < 0.001$ and ****$p < 0.0001$.

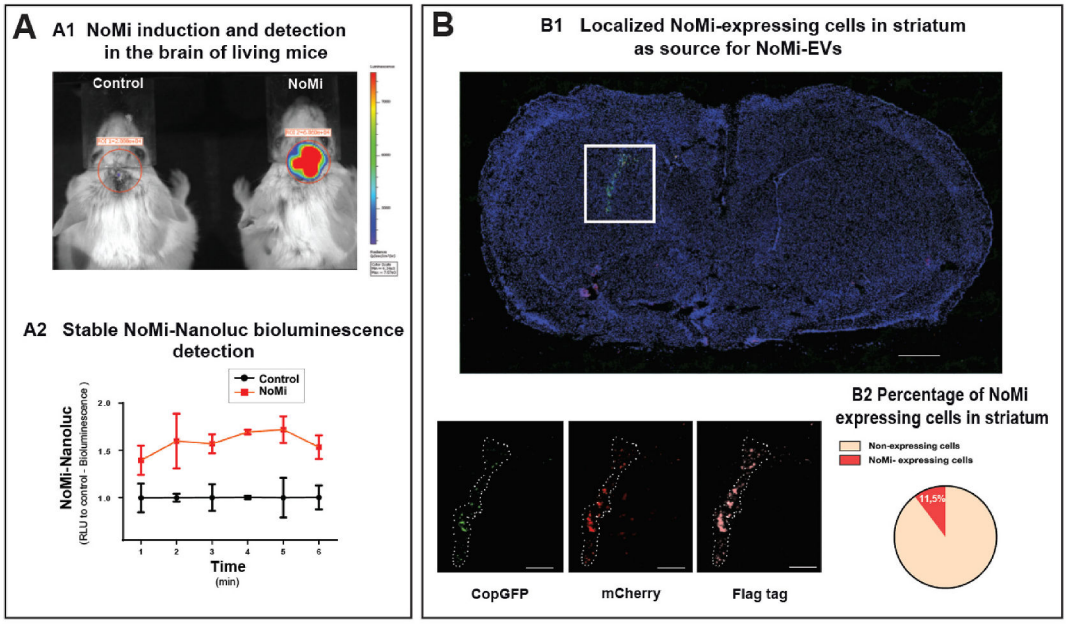

Fig. 5. Local production site of NoMi-EVs in the brain of mice.

(A) NoMi-Nanoluc detection *in vivo* with bioluminescence. [A1] Mice were intracranially injected into the striatum with NoMi-encoding lentiviral vectors (LV) to transduce local brain cells and generate a NoMi-EV source. Thirteen days after brain transduction, NoMi-Nanoluc was detected in the brains of living mice upon intraperitoneal injection of 100 μl of 2 times diluted Nano-Glo® In Vivo Substrate. [A2] NoMi-Nanoluc bioluminescent signal was stable over a timeframe of 6 min (N = 2 controls (injected with 1% PBS/BSA) and N = 2 NoMi (injected with LV encoding NoMi)). (B) Immunofluorescence of coronal sections of NoMi-injected mice. [B1] NoMi-expressing cells in striatum express copGFP, mCherry and anti-Flag tag. [B2] Percentage of NoMi transduced cells in striatum compared to non-transduced cells confirmed local expression of NoMi construct and thus NoMi-EV production. Scale bar 500 μm and 100 μm.

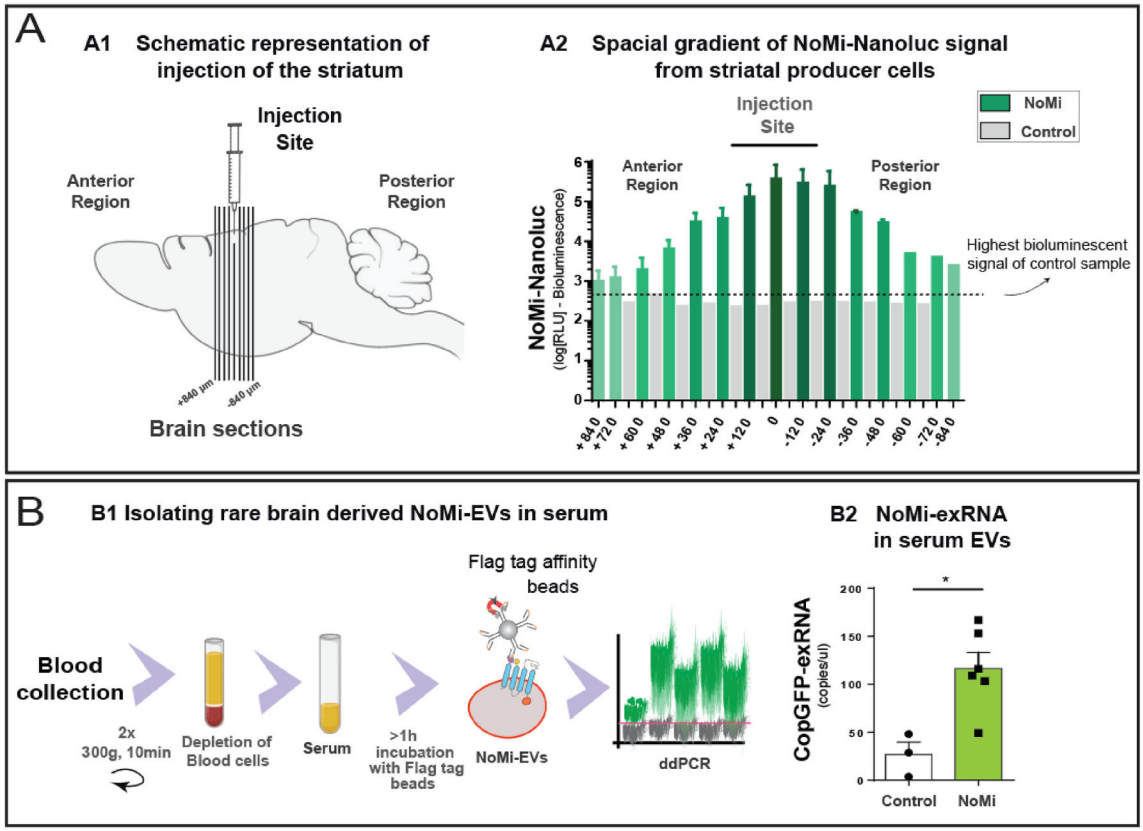

Fig. 6. Detection of rare brain-derived NoMi-EVs in the blood compartment of mice.

(A) NoMi-Nanoluc spatial gradient in striatum. [A1] Intracranial injection of lentivirus encoding NoMi-construct within the striatal region. [A2] A spatial gradient of NoMi-Nanoluc signal was visualized through coronal sections with a peak of luminescence corresponding to the injection site and being lower in both anterior and posterior regions (N = 1 control [injected with 1% PBS/BSA] and N = 3 NoMi [injected with LV encoding NoMi]). (B) Isolation and detection of brain-derived EVs from serum. [B1] Schematic representation of the NoMi-operation in serum EV preparation prior to RNA extraction for digital droplet PCR (ddPCR) analysis. [B2] Confirmation of brain-derived NoMi-EV isolation with copGFP-exRNA amplification and detection by ddPCR (N = 3 control and N = 6 NoMi mice). Data are presented as the mean with SEM (error bars) *p < 0.05. Unpaired *t*-test.

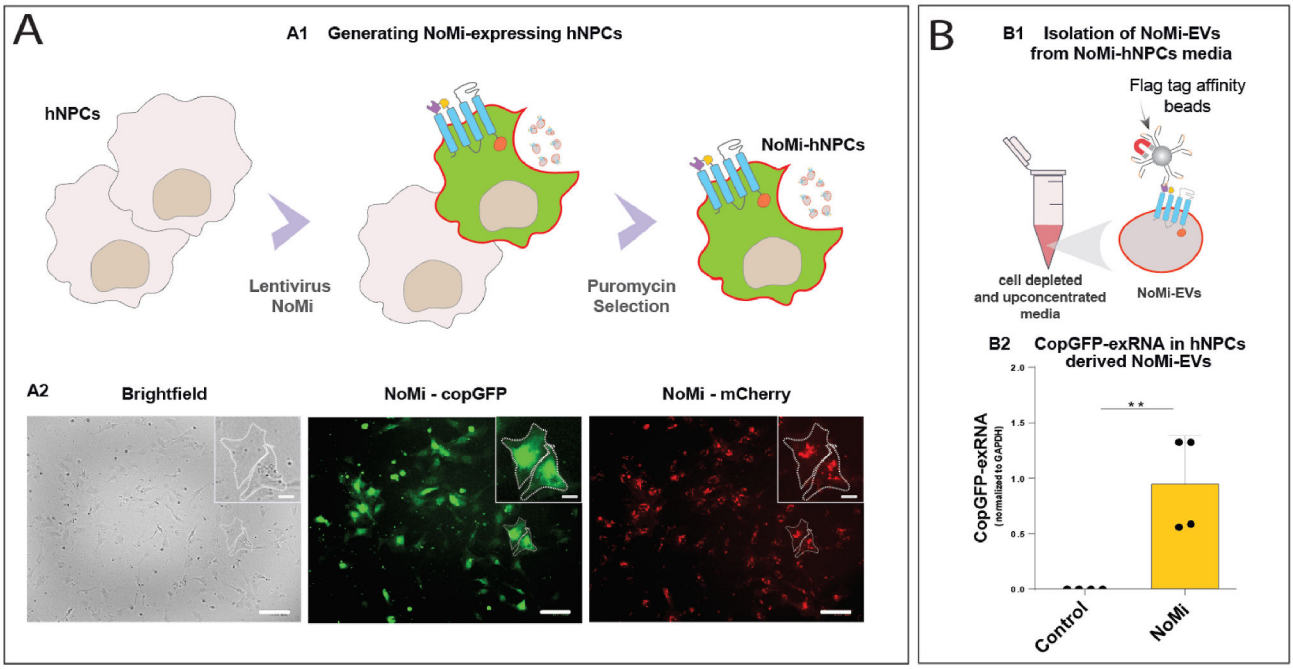

Fig. 7. NoMi-expressing hNPCs secrete NoMi-EVs carrying copGFP exRNAs.

(A) Generation of a stable NoMi-hNPCs culture with NoMi-lentivirus. [A1] Schematic representation of NoMi-hNPCs selection post-transduction with NoMi-lentivirus. [A2] Fluorescent copGFP and mCherry labels from stable transduced NoMi-expressing hNPCs selected with puromycin. Scale bar is 100 μm. (B) Isolation of NoMi-EVs from hNPCs media. [B1] NoMi-hNPCs secrete NoMi-EVs in the media that were pulled down with anti-Flag tag beads. [B2] copGFP-exRNA was detected in NoMi samples by ddPCR and their levels evaluated upon normalization with GAPDH. (N = 4). Data are presented as the mean with SEM (error bars) **$p < 0.01$ Unpaired *t*-test.

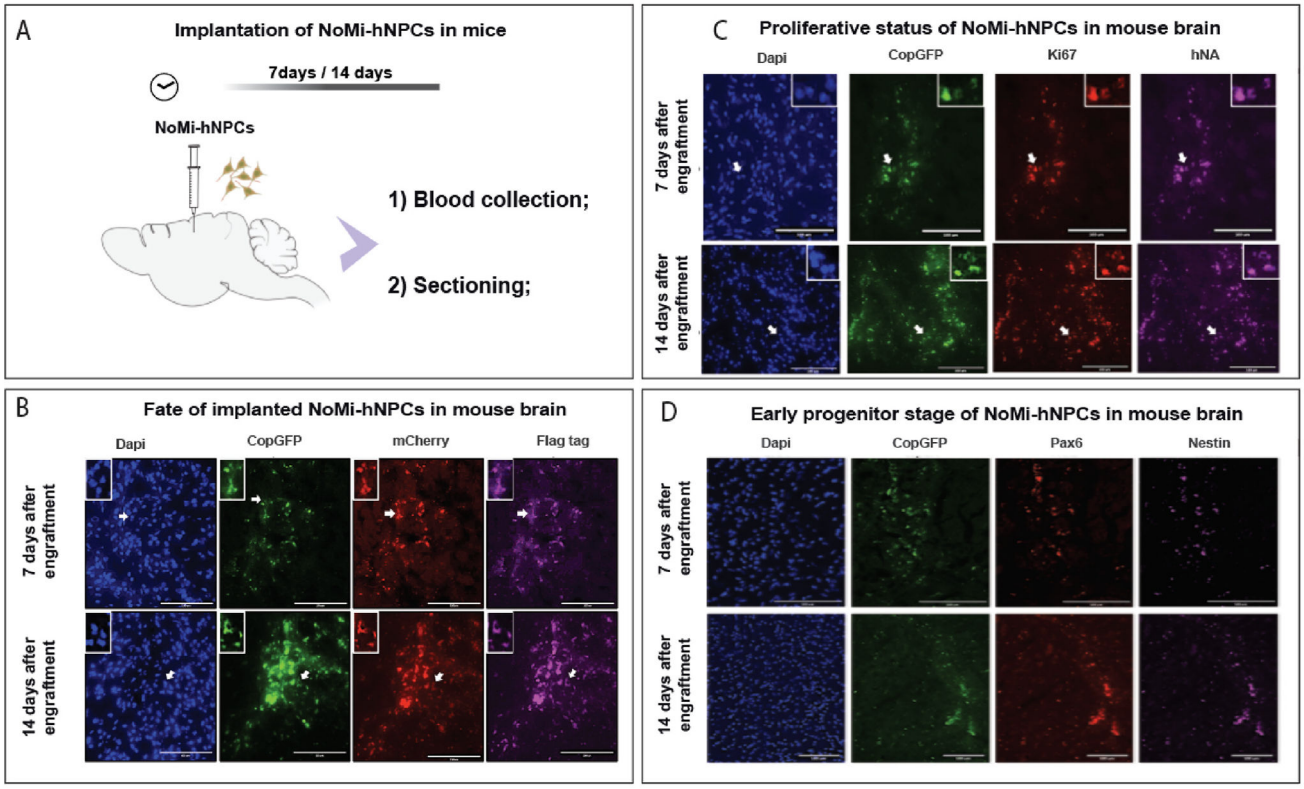

Fig. 8. Human-derived NPCs as a source of NoMi-EVs in the brain of nude mice.

(A) Schematic representation of NoMi-hNPCs implanted in mice. After 7 or 14 days, brains were analyzed for immunofluorescence and serum was collected for NoMi-EV detection (N = 4). (B) NoMi-hNPCs can be distinguished based on NoMi markers such as: copGFP, mCherry (anti-RFP) and Flag tag (anti-Flag tag) at the site of implantation. (C) Ki67 and hNA staining shows non-NoMi encoded features of NoMi-hNPCs implanted in mouse brain, suggesting their ability to proliferate and their human origin, respectively. (D) Pax6 (red) and Nestin (purple) staining shows hNPCs retained their early neural progenitor stage post brain implantation. Immunofluorescence was analyzed with a Keyence BZ-X810 microscope 20x, (N = 4). Scale bar is 100 μm. (For interpretation of the references to colour in this figure legend, the reader is referred to the Web version of this article.)

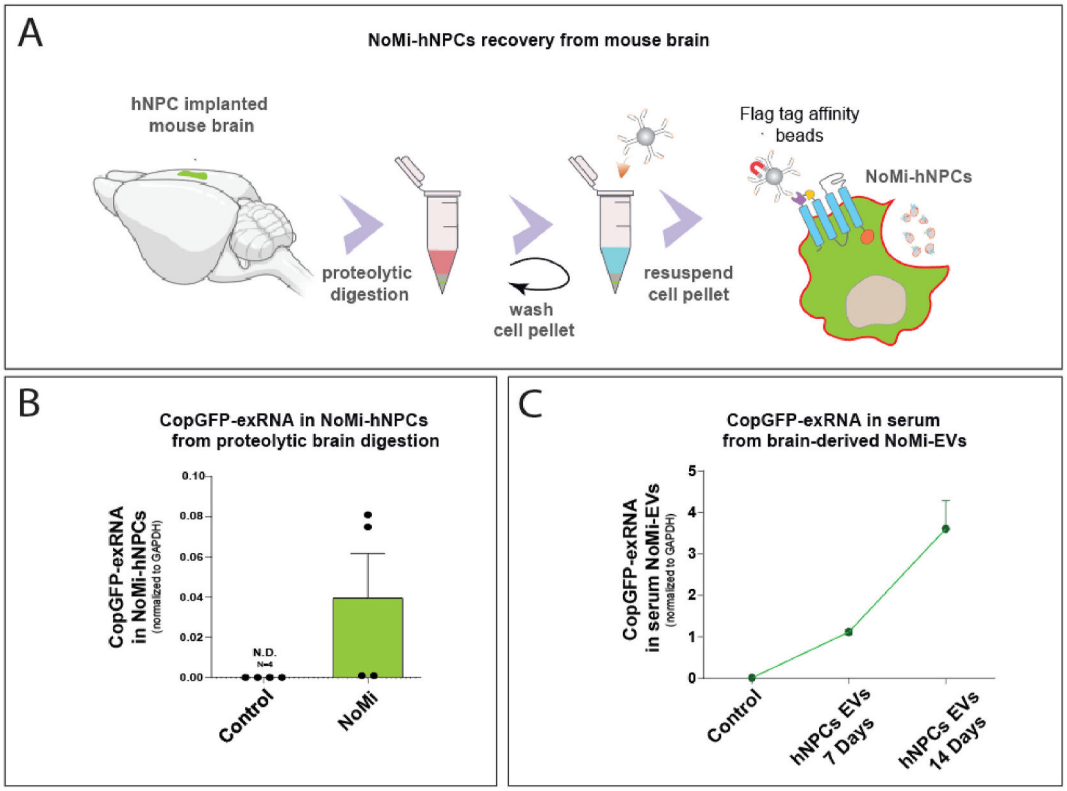

Fig. 9. EVs from implanted NoMi-hNPCs and hNPCs were recovered from mouse brain.

(A) Protocol of recovering of 14-day implanted hNPCs from a mouse brain with the NoMi-operation. (B) CopGFP-exRNA was detected 14 days after implantation of NoMi-hNPCs, after coronal sectioning and proteolytic digestion followed by incubation with anti-Flag beads (N = 4). (C) Brain-derived EVs were isolated from serum 7 and 14 days after NoMi-hNPCs implantation using the NoMi-operation. CopGFP-exRNA in NoMi-EVs was detected by ddPCR with increasing amounts from 7 to 14 days (N = 4, data normalized against GAPDH). Data are presented as the mean with SEM (error bars).